Resource

Cell

Phenotypic Landscape of Schizophrenia-Associated Genes Defines Candidates and Their Shared Functions

Graphical Abstract

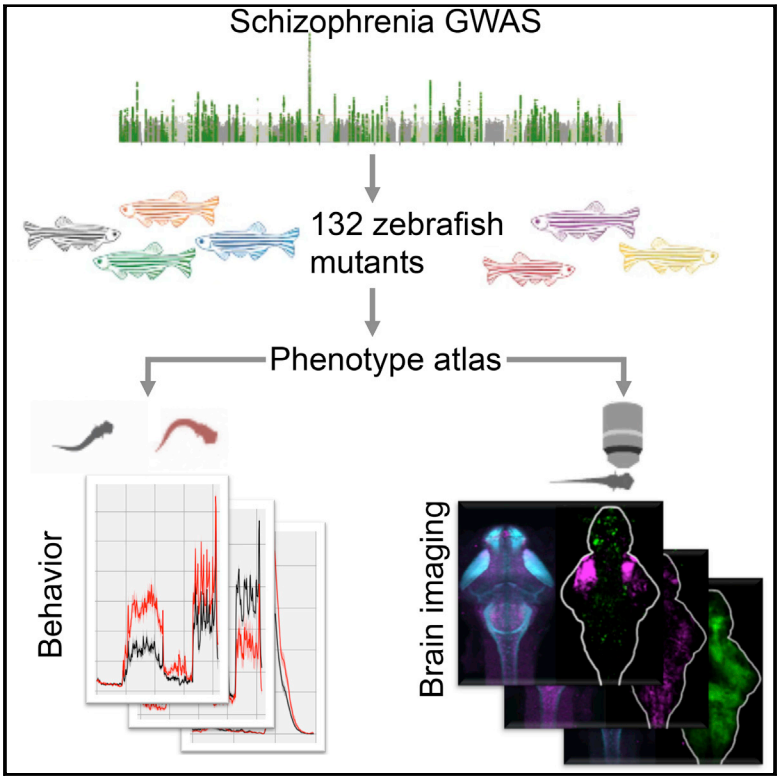

Authors

Summer B. Thyme, Lindsey M. Pieper, Eric H. Li, ..., Joel Greenwood, Steven A. McCarroll, Alexander F. Schier

Correspondence

sthyme@gmail.com (S.B.T.), schier@fas.harvard.edu (A.F.S.)

In Brief

Analysis of zebrafish deficient for human schizophrenia-associated genes generates an atlas of brain and behavior phenotypes for the study of psychiatric disorders.

Highlights

- 132 zebrafish mutants for genes located in schizophrenia-associated genomic regions
- Phenotypes for many understudied genes with previously unknown functions
- Phenotype atlas for abnormal behavior and brain activity
- More than 30 genes prioritized for future study

Thyme et al., 2019, Cell *177*, 478–491
April 4, 2019
https://doi.org/10.1016/j.cell.2019.01.048

CellPress

Cell

Phenotypic Landscape of Schizophrenia-Associated Genes Defines Candidates and Their Shared Functions

Summer B. Thyme,[1,10,*] Lindsey M. Pieper,[1] Eric H. Li,[1] Shristi Pandey,[1] Yiqun Wang,[1] Nathan S. Morris,[1] Carrie Sha,[1] Joo Won Choi,[1] Kristian J. Herrera,[1] Edward R. Soucy,[2] Steve Zimmerman,[1] Owen Randlett,[1] Joel Greenwood,[2] Steven A. McCarroll,[3,4,5] and Alexander F. Schier[1,2,3,6,7,8,9,*]

[1]Department of Molecular and Cellular Biology, Harvard University, Cambridge, MA 02138, USA
[2]Center for Brain Science, Harvard University, Cambridge, MA 02138, USA
[3]Broad Institute of MIT and Harvard, Cambridge, MA 02142, USA
[4]Department of Genetics, Harvard Medical School, Boston, MA 02115, USA
[5]Stanley Center for Psychiatric Research, Cambridge, MA 02142, USA
[6]Biozentrum, University of Basel, CH-4056 Basel, Switzerland
[7]Harvard Stem Cell Institute, Cambridge, MA 02138, USA
[8]FAS Center for Systems Biology, Harvard University, MA 02138, USA
[9]Allen Discovery Center for Cell Lineage Tracing, Seattle, WA 98104, USA
[10]Lead contact
*Correspondence: sthyme@gmail.com (S.B.T.), schier@fas.harvard.edu (A.F.S.)
https://doi.org/10.1016/j.cell.2019.01.048

SUMMARY

Genomic studies have identified hundreds of candidate genes near loci associated with risk for schizophrenia. To define candidates and their functions, we mutated zebrafish orthologs of 132 human schizophrenia-associated genes. We created a phenotype atlas consisting of whole-brain activity maps, brain structural differences, and profiles of behavioral abnormalities. Phenotypes were diverse but specific, including altered forebrain development and decreased prepulse inhibition. Exploration of these datasets identified promising candidates in more than 10 gene-rich regions, including the magnesium transporter *cnnm2* and the translational repressor *gigyf2*, and revealed shared anatomical sites of activity differences, including the pallium, hypothalamus, and tectum. Single-cell RNA sequencing uncovered an essential role for the understudied transcription factor *znf536* in the development of forebrain neurons implicated in social behavior and stress. This phenotypic landscape of schizophrenia-associated genes prioritizes more than 30 candidates for further study and provides hypotheses to bridge the divide between genetic association and biological mechanism.

INTRODUCTION

Neuropsychiatric disorders are highly heritable. The understanding of their underlying genetic predispositions has recently accelerated, providing new opportunities to decipher disease mechanisms and discover potential drug targets. However, progress has been limited in part because the dozens of loci associated with these disorders contain hundreds of candidate genes (Schizophrenia Working Group of the Psychiatric Genomics Consortium, 2014). In particular, single-nucleotide polymorphisms (SNPs) linked by genome-wide association study (GWAS) only define disease-associated genomic regions, which often span many genes (of which the culpable genes are unknown) or might include regulatory elements for distant genes (Won et al., 2016). Many of the same risk loci are also associated with multiple neuropsychiatric disorders (Cross-Disorder Group of the Psychiatric Genomics Consortium, 2013; Gandal et al., 2018) and even sleep disorders (Lane et al., 2017). This shared genetic predisposition indicates that some genes may contribute generally to brain health and development, while others may influence specific dimensions of disease manifestations.

One of the richest of association datasets exists for schizophrenia (Schizophrenia Working Group of the Psychiatric Genomics Consortium, 2014). In 2014, the Schizophrenia Working Group of the Psychiatric Genomics Consortium identified 108 genomic loci at which common variants significantly associated with the disorder. Some identified genes align with hypotheses from previous research: for example, the implication of dopamine receptor D2 (*DRD2*, the target of many antipsychotic medications) may align with the dopamine hypothesis. The largest association signal, in the major histocompatibility complex (MHC) locus, appears to arise in part from the complement component 4 genes, which might contribute to excessive synaptic pruning (Sekar et al., 2016). However, many associated genes have not been studied, particularly in the context of nervous system development and activity.

To discover the mechanisms underlying polygenic illnesses such as schizophrenia and other neuropsychiatric disease, it would be useful to identify the *in vivo* functions of many associated genes; such analysis could also prioritize candidate genes for further analyses. We reasoned that zebrafish, a small and

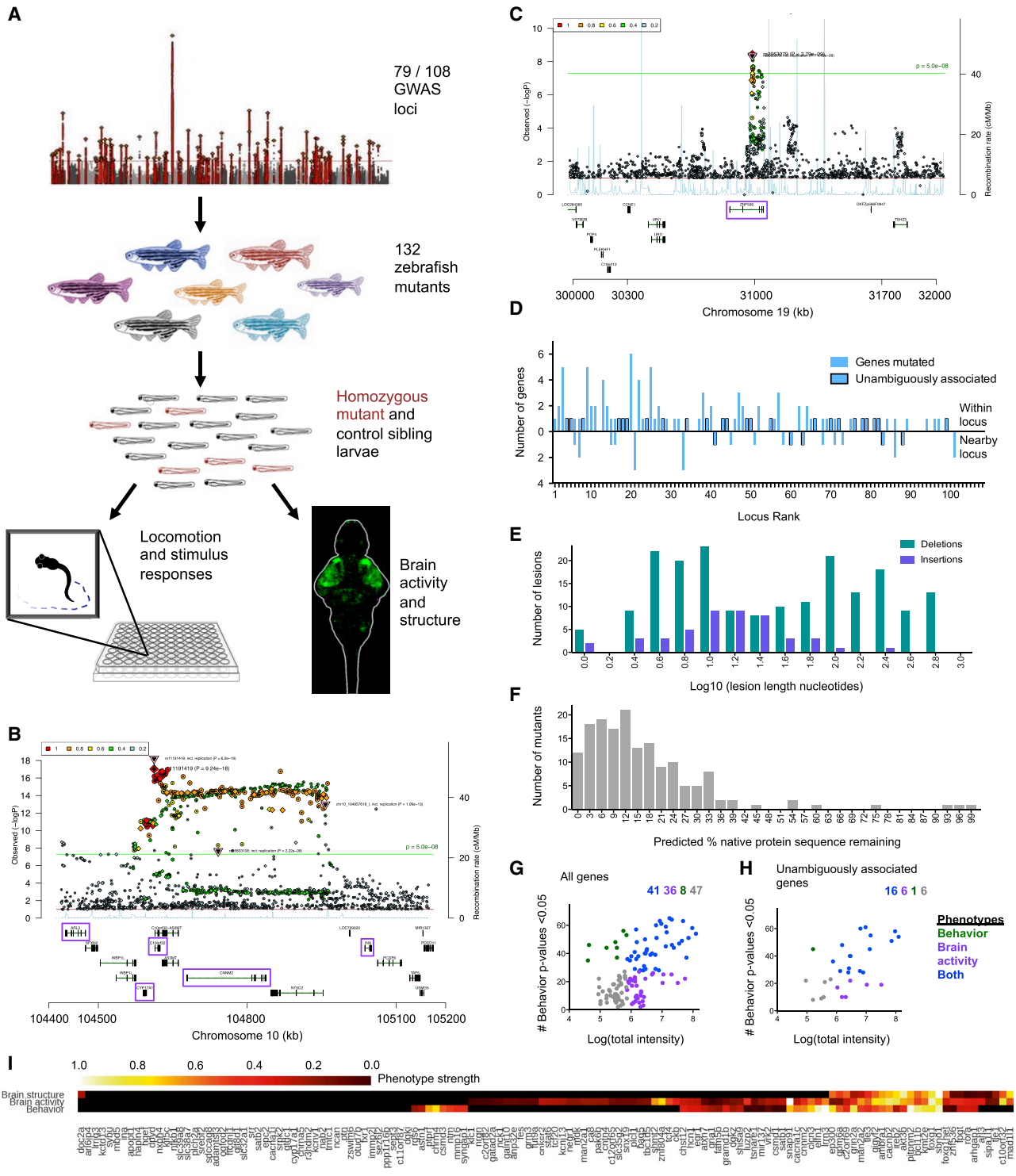

Figure 1. Generation and Analysis of 132 Mutants for Schizophrenia-Associated Genes

(A) Mutants were generated via Cas9 mutagenesis for genes found within and neighboring genomic loci linked to schizophrenia through genome-wide association. Manhattan plot image was adapted from Schizophrenia Working Group of the Psychiatric Genomics Consortium (2014). The resulting mutants were assessed for changes to brain morphology, brain activity, and behavior. Multiple zebrafish orthologs existed for 33 of the 132 genes (165 individual zebrafish genes), and both copies were mutated and assessed together.

(B) Ricopili plot (https://data.broadinstitute.org/mpg/ricopili/) for multi-gene locus #3 of 108 from which five candidates (purple boxes) were selected for mutagenesis.

(legend continued on next page)

low-cost vertebrate (Rennekamp and Peterson, 2015; Rihel et al., 2010), could be used to analyze orthologs of associated genes and that comprehensive mutant phenotyping could identify relevant candidates and suggest their impacts on brain function (Figure 1A). Although human neuropsychiatric illness cannot be phenocopied in zebrafish, and homozygous knockouts differ from the functionally subtle polymorphisms that commonly segregate in human populations, neuroanatomical and behavioral phenotypes relevant to human biology can be scored in zebrafish (Burgess and Granato, 2007b; Meincke et al., 2004; Rihel et al., 2010; Wilson et al., 2002). Previous studies have shown that zebrafish are a powerful model system to uncover developmental and behavioral functions of human genes (Escamilla et al., 2017; Haesemeyer and Schier, 2015; Hoffman et al., 2016). The two organisms share the majority of genes and tissues, including homologous brain structures (Wilson et al., 2002), and mutant screens have defined the functions of hundreds of conserved genes (Driever et al., 1996; Haffter et al., 1996; Kettleborough et al., 2013). Moreover, mutant analyses in zebrafish have yielded important insights into pathways underlying human neuropsychiatric illness (Escamilla et al., 2017; Hoffman et al., 2016).

To identify neurobiological functions and define candidate genes, we created mutants for 132 schizophrenia-associated genes and performed large-scale phenotypic analyses of brain activity, morphology and behavior. We established phenotypic databases, websites to share these datasets (genepile.com/scz_gwas108 and stackjoint.com/zbrain) (Video S1), and robust analysis tools to facilitate large-scale studies. Guided by these datasets, we identified promising candidates in multi-gene loci and discovered neurobiological roles for more than 30 genes, including several that were largely understudied.

RESULTS

Generation of 132 Mutants for Schizophrenia-Associated Genes

We focused on the 108 genomic loci at which common variants exhibited genome-wide significant associations in the largest schizophrenia case/control analysis (Schizophrenia Working Group of the Psychiatric Genomics Consortium, 2014), choosing 132 genes to mutate and phenotype in zebrafish (Figure 1A, Table S1, Table S2). For gene-rich loci, numerous candidate genes were individually mutated (Figure 1B). Criteria for choosing genes to mutate included nervous system expression (Lein et al., 2007) and human data that further implicated them in neuropsychiatric illness, such as patient exome sequencing or postmortem brain analyses of gene expression or chromatin conformation (Fromer et al., 2016; Won et al., 2016). While some candidates had known neurobiological functions, we mutated many minimally studied genes based only on nervous system expression (Table S1). Twenty-nine of the 132 genes were strongly implicated by multiple lines of previous research or were the only candidate within and neighboring their respective locus (Figure 1C), and therefore were considered "unambiguously associated" with schizophrenia (Figure 1D, Table S1). These included well-known genes such as calcium channel subunits and the NMDA receptor subunit *grin2a*, minimally characterized brain-expressed candidates from single-gene loci such as *znf536* (Figure 1C) and *znf804a*, and genes implicated by CommonMind postmortem patient brain expression data (Fromer et al., 2016) such as *clcn3* and *snap91*. Selected genes were not always closest to the association signal. For example, at locus 83 we mutated *foxg1*, even though it is almost 1 megabase from the associated region, instead of the closer *prkd1* because (1) the region overlaps with a known *FOXG1* enhancer (Allou et al., 2012) active in human neural progenitors (Won et al., 2016), (2) *foxg1* regulates forebrain development (Eagleson et al., 2007; Roth et al., 2010), and (3) this factor is involved in multiple neurodevelopmental disorders (Mariani et al., 2015). The criteria for gene choices at every locus are described in Table S1.

We used Cas9 and multiple guide RNAs (gRNAs) to mutagenize a conserved part of each protein near the N terminus, predicted to result in substantial truncations (Figure 1E, Figure 1F, genepile.com/scz_gwas108). Only two homozygous mutants, *cacna1c* and *slc32a1* (Stainier et al., 1996; Wojcik et al., 2006), were lethal prior to 6 days post-fertilization (dpf). An additional

(C) Ricopili plot for a gene (*znf536*) considered unambiguous because there are no other genes within 0.5 megabase on each side of the associated region, and the gene within the association region is brain-expressed.

(D) Mutants made from 79 of 108 associated genomic loci. The locus rank reflects the statistical strength of the genetic association, with 1 being the most significantly associated. A region of 0.5–2 MB around each locus was analyzed, and genes outside of the region of linkage disequilibrium were selected for 19 of the 79 loci. Unambiguously associated genes are implicated strongly by previous literature, such as genes involved in glutamatergic neurotransmission, or are the only genes within or neighboring their locus (Table S1).

(E) Mutations generated from Cas9 cleavage. Some mutant alleles consisted of several lesions if multiple gRNAs cleaved the genome independently, and all are included here. A range of mutations was recovered, tending to be either small (<15 bases) when a single gRNA cleaved or large (>100 bases) when a deletion spanned target sites of multiple gRNAs.

(F) Protein sequence predicted to remain in mutants, based on sequence alignment identity. This analysis included both orthologs if the gene was duplicated (33 genes), for a total of 165 individual genes (163 in graph, as it does not include *mir137* and one gene with unclear wild-type protein sequence length). The four mutants with >75% of the protein remaining did not have frameshifting mutations but did have phenotypes (Table S2), indicating that the protein function was disrupted.

(G) Phenotypes in all 132 mutants based on analysis of brain activity signals and 71 behavioral assessments. See also Figure S1 and Figure S2 for the cutoffs for classifying which mutants have phenotypes.

(H) Phenotypes in mutants for the 29 unambiguously associated genes (Table S1).

(I) Phenotype dimensions affected in mutants for 132 genes from 79 schizophrenia-associated loci. Quantification of brain activity, brain structure, and behavioral differences for mutants designated as having a phenotype (Figure S1, Figure S2, Figure 1G, Figure 3B, Table S2) was scaled for comparison between the three measures, with the weakest phenotype designated as 0 and strongest as 1. Measures below the cutoff for phenotype designation (Figure S1, Figure S2) are displayed in black.

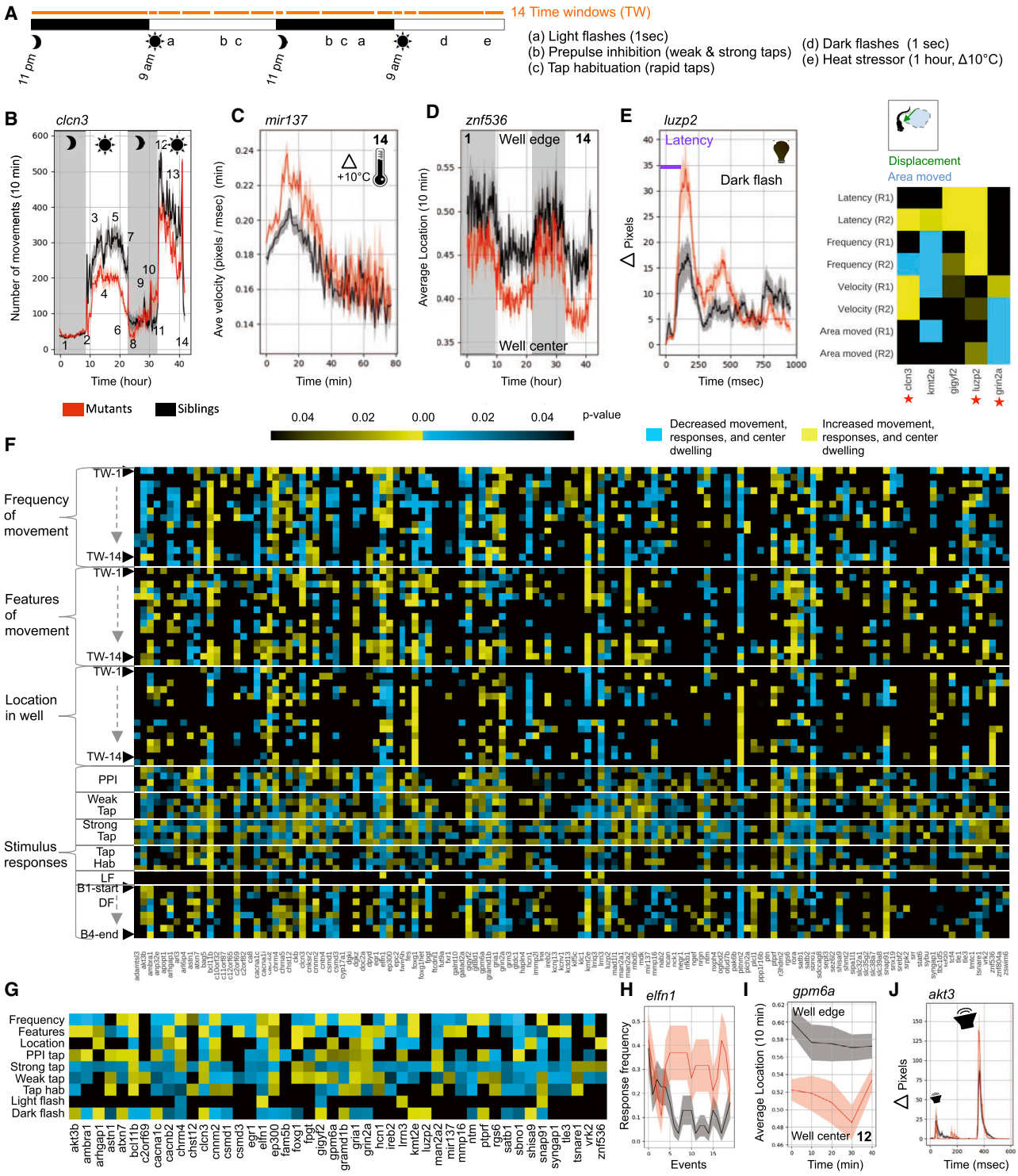

Figure 2. Behavioral Phenotypes in Zebrafish Mutants

(A) Behavioral assay protocol. Frequency of movement, features of movement, and location preferences were calculated for each of 14 windows of the data (see STAR Methods for description of each time window). Stimulus responses were quantified from high-speed (285 frames-per-second) 1 s long movies. The exact stimulus paradigms are described in the STAR Methods. Behavioral testing was repeated for 73 of the 132 mutants, 46 of those designated as having a phenotype (Figure S1, Figure S2).

(B). Example of altered frequency of movement for *clcn3* -/- mutants compared to +/- sibling controls for entire protocol (time windows 1-14), including the approximate location of each time window. P value = 0.005; N = 32 +/- , 33 -/-.

(legend continued on next page)

24 zebrafish mutants (18%) were lethal or underdeveloped by adulthood but appeared healthy at 6 dpf (Table S2). At this larval stage the animal is small enough for high-throughput studies, has complex behaviors (e.g., hunting, sleeping, learning, navigating), and major adult neuron types are present (Pandey et al., 2018). More than half of all mutants had phenotypes in brain activity or behavior (Figure 1G, Table S2, Figure S1, Figure S2), including more than 75% of those for unambiguously associated genes (Figure 1H). The presence and severity of brain activity and behavioral phenotypes were often, but not always, correlated (Figure 1G, Figure 1I).

Baseline Behavior and Sensory Stimulation

To uncover both baseline and stimulus-driven behavioral abnormalities, we subjected over 15,000 larvae from 132 mutants (Table S2) to a range of behavioral paradigms from 4–6 dpf (Figure 2A). We assessed baseline motion over multiple day-night cycles and responses to sensory stimulation. Phenotypic assays compared homozygous mutants to heterozygous and/or wild-type siblings and all larvae were genotyped after assays. As it was unknown how perturbing these genes would manifest in larval zebrafish behavior, we developed software to measure a comprehensive range of parameters for both baseline movement and stimulus responses (for details see STAR Methods, Table S3). We determined the frequency of movement (Figure 2B), features of movement (e.g., velocity, distance traveled) (Figure 2C), and location preference within the well (Figure 2D). These baseline parameters were calculated for 14 different time windows over the 2-day experiments (Figure 2A) to distinguish phenotypes that change over time, such as sleep-like behavior. Sensory stimulation included response to light flash (Burgess and Granato, 2007a), dark flash (Wolman et al., 2011), and acoustic tap, as well as habituation to taps (Wolman et al., 2011), prepulse inhibition (Burgess and Granato, 2007b), and movement during a period of heat. For startle responses to a stimulation event, such as a dark flash, multiple parameters of the response motion (e.g., speed, displacement) were calculated in addition to frequency of the response (Figure 2E).

We discovered mutants with phenotypes in each behavioral paradigm (Figure 2F, genepile.com/scz_gwas108). Many mutants were affected in multiple assays (Figure 2F, Figure 2G, Table S4, Figure S3, Figure S4), although there were exceptions, such as mutants for the uncharacterized and unambiguously associated leucine zipper protein *luzp2*, which exhibited increased dark flash responses and no changes to baseline motion parameters (Figure 2E, Figure 2G). Our fine-grained analysis method identified mutants with abnormalities in specific modalities of stimulus response, such as response latency or velocity (Figure 2E). Similarly, some mutants had subtle differences in a specific attribute of their baseline motion, such as the increased velocity of movements in *mir137* mutants that was accentuated by heat (Figure 2C). Other distinct phenotypes included increased light responsiveness in *elfn1* mutants (Figure 2H), decreased prepulse inhibition in *atxn7* mutants (Figure 2G), and a strong preference for the well center in *znf536* mutants (Figure 2D). Behavioral differences in zebrafish mutants also mirrored mammalian behavioral phenotypes. For example, the *gpm6a* mutant zebrafish preferred the well center reminiscent of *Gpm6a* mutant mice, which avoid closed spaces (El-Kordi et al., 2013) (Figure 2I), and mutants for *akt3* displayed decreased prepulse inhibition in zebrafish (Figure 2J), as also seen in mouse models (Bergeron et al., 2017). These *in vivo* datasets reveal the immense diversity of behavioral changes caused by mutations in schizophrenia-associated genes and provide entry points to study the underlying neural circuits.

(C) Example of altered features of movement for time window 14. p value = 0.001; N = 36 +/- , 32 -/-.

(D) Example of altered location preference for entire protocol (time windows 1 to 14). P value = 0.001; N = 17 +/- , 18 -/-.

(E) Example of a stimulus-driven high-speed response to a one second dark flash, and quantification of dark flash phenotypes across various modalities of the response. The response graph is an average of larvae in the mutant and control groups for events where a response was observed. Dark flash responses were analyzed for four hour-long blocks of dark flashes by assessing the first ten and last ten flashes each block, totaling eight separate statistical analyses. These eight p values were combined using Fisher's method to generate the heatmap of the five mutant phenotypes. Merged p value for dark flash section (first ten flashes of block 4) for *luzp2* = 0.02 (p values are not calculated for stimulus response traces), with latency being the most significant contributing metric with p value = 0.0007; N = 32 +/- , 35 -/-.

(F) Summary of all 71 behavioral assays for all tested mutants. If a mutant was tested more than once, the lowest combined p value is shown here. If multiple comparisons were made for a given gene, such as in the case of duplicated genes, the lowest p value is shown. Significant results are reported for time windows (TW) 1-14 and the significance for the entire protocol (position 15 in heatmap) for each of the slower speed measurements. For high-speed stimulus responses, results presented in the heatmap are as follows: PPI (day early prepulse, e.g., responses in first 20 min of stimulus block, about 10-15 events; day all prepulse, e.g., all responses; night early prepulse; night all prepulse), Weak Tap (day early; day all; night early; night all), Strong Tap (day early; day all; night early; night all), Tap Habituation (day block 1; day block 2; day block 3; night block), Light flash (day; night), Dark Flash (block 1 start, e.g., first 10 flashes of 60 min block; block 1 end, e.g., last 10 flashes of 60 min block; block 2 start; block 2 end; block 3 start; block 3 end; block 4 start; block 4 end). Specific examples of raw metrics for every mutant are available on genepile.com/scz_gwas108.

(G) The 46 mutants shown here had a total behavioral phenotype score greater than the cutoff (Figure S2) and were tested more than once. If the merged p value (Figure S2) for the assay was significant ($p < 0.05$) between two independent repeats, the phenotype was counted and the lowest p value of the two is displayed. Otherwise neither p value was included. The significant phenotype had to be in the same time window or in the same stimulus assay to be counted (e.g., a significant phenotype observed on night 1 in one repeat and night 2 in another was not counted). Specific examples of raw metrics of the repeatable phenotypes for these 46 mutants are available on genepile.com/scz_gwas108. See also Figure S2.

(H) The *elfn1* mutants displayed increased responses to light stimulation. Merged p value for day light flashes = 0.009 with 8/15 significant metrics, although the displayed frequency metric is itself non-significant; N = 31 +/- ;+/-, 19 -/-;-/-.

(I) The *gpm6a* mutants displayed a preference for the well center. P value = 0.002; N = 19 +/- ;+/-, 11 -/-;-/-.

(J) The *akt3* mutants displayed reduced prepulse inhibition. The mutant response profile demonstrates the prepulse behavioral paradigm and response, where a weak tap (prepulse) is followed 300 ms later by a strong tap. Merged p value for the day early prepulse section = 0.018 with 10/36 significant metrics; N = 23 +/+ and +/- , 10 -/-. Plots of mutant compared to control groups in all panels represent mean ± SEM. See also Figure S3. See also Figure S4.

Whole-Brain Activity and Morphology

To detect altered brain activity and morphology in the 132 mutants, we imaged more than 10,000 6 dpf larvae brains (Table S2). Phenotypic assays compared homozygous mutants to heterozygous and/or wild-type siblings, and all larvae were genotyped after assays. Whole-brain activity of unstimulated freely swimming larvae was determined by measuring the levels and distribution of phospho-ERK (Randlett et al., 2015), a downstream reporter of calcium signaling. Imaged brains were registered to the Z-Brain atlas and significant changes in activity between mutant and control groups were calculated (Randlett et al., 2015). Changes in brain volume in zebrafish mutants were calculated using deformation-based morphometry (Rohlfing and Maurer, 2003). All brain activity and structure maps can be explored in our website resource, stackjoint.com/zbrain, where users can also upload and share their own imaging data (Video S1).

Only 16 (12%) of the mutants had substantial brain morphological differences (Figure 3A, Figure 3B, Table S2), compared to over half with brain activity differences (Figure 1G). Mutants for the transcription factors *foxg1* and *bcl11b* (Ctip2) had smaller forebrains (Figure 3C), consistent with their known roles in mouse forebrain development (Chen et al., 2008; Eagleson et al., 2007). Similarly, *rora* transcription factor mutants had underdeveloped cerebella (Sidman et al., 1962), and *akt3* mutants had overall smaller brains (Easton et al., 2005). Thus, mutant brain anatomy differences agreed with previously described mammalian models. New neurodevelopmental roles were uncovered for lesser-studied genes such as the translational repressor *gigyf2* (Guella et al., 2011; Kryszke et al., 2016; Morita et al., 2012) and the transcription factor *znf536,* mutants for which both had decreased volume in specific brain subregions including the forebrain (Figure 3C), and histone methyltransferase *kmt2e* mutants (Ali et al., 2013) (Table S2, stackjoint.com/zbrain), which had increased brain volume (Figure 3C). Mutant brain structure phenotypes often did not spatially correlate with the expression patterns of the mutated genes (Figure 3D, stackjoint.com/basic), as exemplified by the widespread expression of *bcl11b*, *rora*, and *znf536* and their localized volume loss (Figure 3C).

The neuroanatomical screen also highlighted genes of relevance to multiple neuropsychiatric disorders beyond schizophrenia (Cascella et al., 2009; Gandal et al., 2018). For example, we mutated several genes linked to autism as well as schizophrenia. The histone methyltransferase *kmt2e* (schizophrenia locus 52 of 108) is strongly associated with autism through GWAS (Grove et al., 2019) and has been highlighted as a *de novo* mutation in patients (Dong et al., 2014). The increase in *kmt2e* mutant brain size was unique to this gene, as the other 15 mutants with substantial morphological differences mainly had reduced volume (stackjoint.com/zbrain). Increased brain volume is also observed in some autistic patients (Redcay and Courchesne, 2005). The discovery of phenotypes that extend beyond schizophrenia highlights the utility of this resource for catalyzing future studies in several fields (Table S1).

More than half of the mutants had brain activity phenotypes (Figure 1G, Figure 4), including 75% of genes unambiguously associated with schizophrenia (Figure 1H, Table S1). Decreased and increased activity differences emerged in both broad and localized patterns (Figure 4A, Figure 4B, Table S2, stackjoint.com/zbrain). Although the molecular pathways underlying schizophrenia are largely unresolved, glutamatergic neurotransmission, calcium channels, and synaptic pruning are highly implicated (Heyes et al., 2015; Schizophrenia Working Group of the Psychiatric Genomics Consortium, 2014; Sekar et al., 2016). Our approach uncovered whole-brain activity phenotypes for genes associated with these functionalities (Figure 4A) as well as others with completely unknown functions (Figure 4B), such as *luzp2* (leucine zipper protein 2) and *gramd1b* (GRAM domain containing 1B). The unambiguously associated complement pathway regulator *csmd1* exhibited broad activity increases. Elevated complement component 4 levels are observed in schizophrenia patients and may contribute to aberrant synaptic pruning (Sekar et al., 2016). In contrast, mutants for two unambiguously associated ion channel genes, *cacna1c* (Stainier et al., 1996) and *clcn3*, had localized forebrain activity decreases. Gene expression did not always spatially correlate with brain activity (Figure S5, stackjoint.com/basic), just as for structural phenotypes (Figure 3D), and in some cases was not even observed in the brain areas with significant activity changes (*cnnm2b,* Figure S5).

To quantitatively determine whether the same brain regions were affected across different mutants, we calculated the overlap in signal between the mutant brain activity maps (Figure 4C). Hierarchical clustering of signal overlap uncovered spatial relationships between the brain areas affected in mutants. For example, the genes *clcn3* and *cacna1c* (Figure 4A) both had signal in the pallium region of the forebrain (Figure 4D, label 2). Shared signals (Table S5) ranged from highly region-specific such as the olfactory bulb (Figure 4E, label 1) to widespread effects (Figure 4E, label 5). Unambiguously associated genes (red stars) were more likely to have overlapping signals. For example, mutants with signals mainly in the pallium (label 2) were all unambiguously associated, including *bcl11b*, *gria1*, *znf536*, *clcn3*, and *cacna1c.* Several other mutants, such as *rora* and *shmt2* (Figure 4F), had activity changes in the pallium but were not part of the pallium cluster, since they also had changes in the other commonly affected brain region: retinal arborization field AF7 and tectum (Figure 4E, label 4). Retinal arborization field AF7 (blue arrow) is one of ten arborization fields and is a visual brain area that is specifically activated during hunting (Semmelhack et al., 2014). Mutants in which this region was affected also displayed corresponding activity changes in a specific subregion of the hypothalamus, indicative of a functional connection between the two areas (stackjoint.com/zbrain). The molecular roles of genes in the tectal cluster (Figure 4E, label 4) were diverse, ranging from transcriptional regulation (*tcf4*, *znf804a*) to glutamatergic neurotransmission (*grin2a*, *elfn1*) to protein glycosylation (*man2a2*). Thus, the brain morphology and activity atlases not only uncover a large diversity of phenotypes caused by mutations in schizophrenia-associated genes but also reveal unexpected anatomical convergences despite distinct molecular functions of the mutated genes.

Narrowing Down Candidates in Multi-Gene Loci

Comparisons between phenotypes of mutants within multigene loci nominated candidates for stronger consideration and

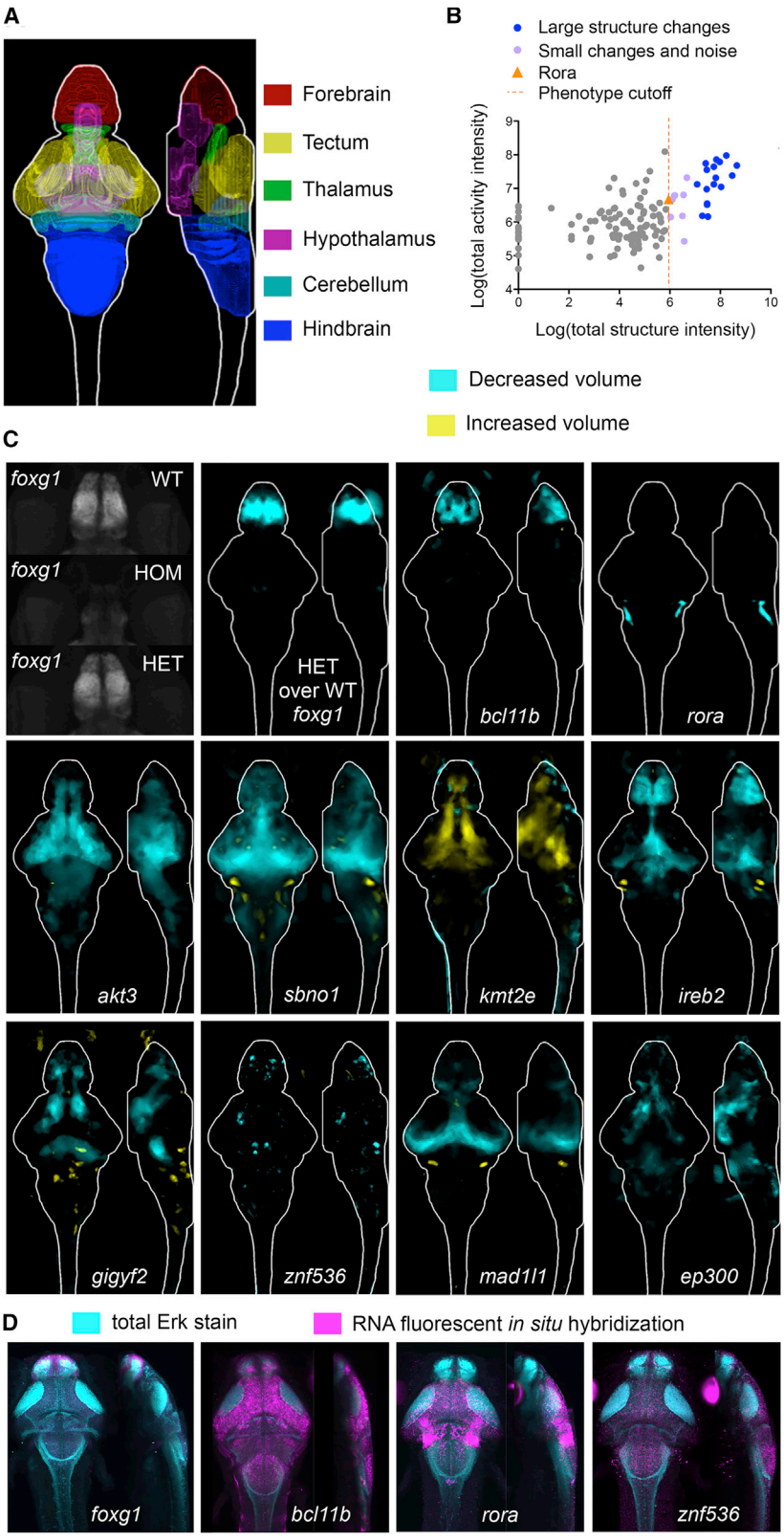

Figure 3. Whole-Brain Morphology Phenotypes in Zebrafish Mutants

(A) Location of several major regions in the zebrafish brain (Randlett et al., 2015).

(B) Comparison between brain activity and morphology data for all mutants. The *rora* mutant (orange triangle) represents the smallest (5.95) structural change designated as a phenotype, shown in panel C. Small signals that were not symmetrical were considered noise, compared to small but symmetrical changes as observed in the *rora* mutant.

(C) Examples of structural differences in mutants calculated using deformation-based morphometry and displayed as sum-of-slices projections (Z- and X- axes). Brain images represent the significant differences in signal between two groups (Randlett et al., 2015), most often homozygous mutants versus heterozygous and/or wild-type siblings (Table S2). The number of animals used in all imaging experiments is available in Table S2 and on stackjoint.com/zbrain (website naming conventions for datasets described in STAR Methods). Brain maps were averaged from two independent clutches of larvae if the experiment was repeated and irreproducible signals were eliminated (STAR Methods). Raw imaging data examples (maximum projections) are shown for the *foxg1* mutants, demonstrating that the forebrain in homozygous (HOM) mutants is underdeveloped. A reduction in forebrain size of heterozygous (HET) *foxg1* mutants when compared to wild-type (WT) siblings can be quantified with deformation-based morphometry (sum-of-slices projection), although it is not readily apparent in the raw projection.

(D) Fluorescent RNA *in situ* images for four mutants with altered brain morphology.

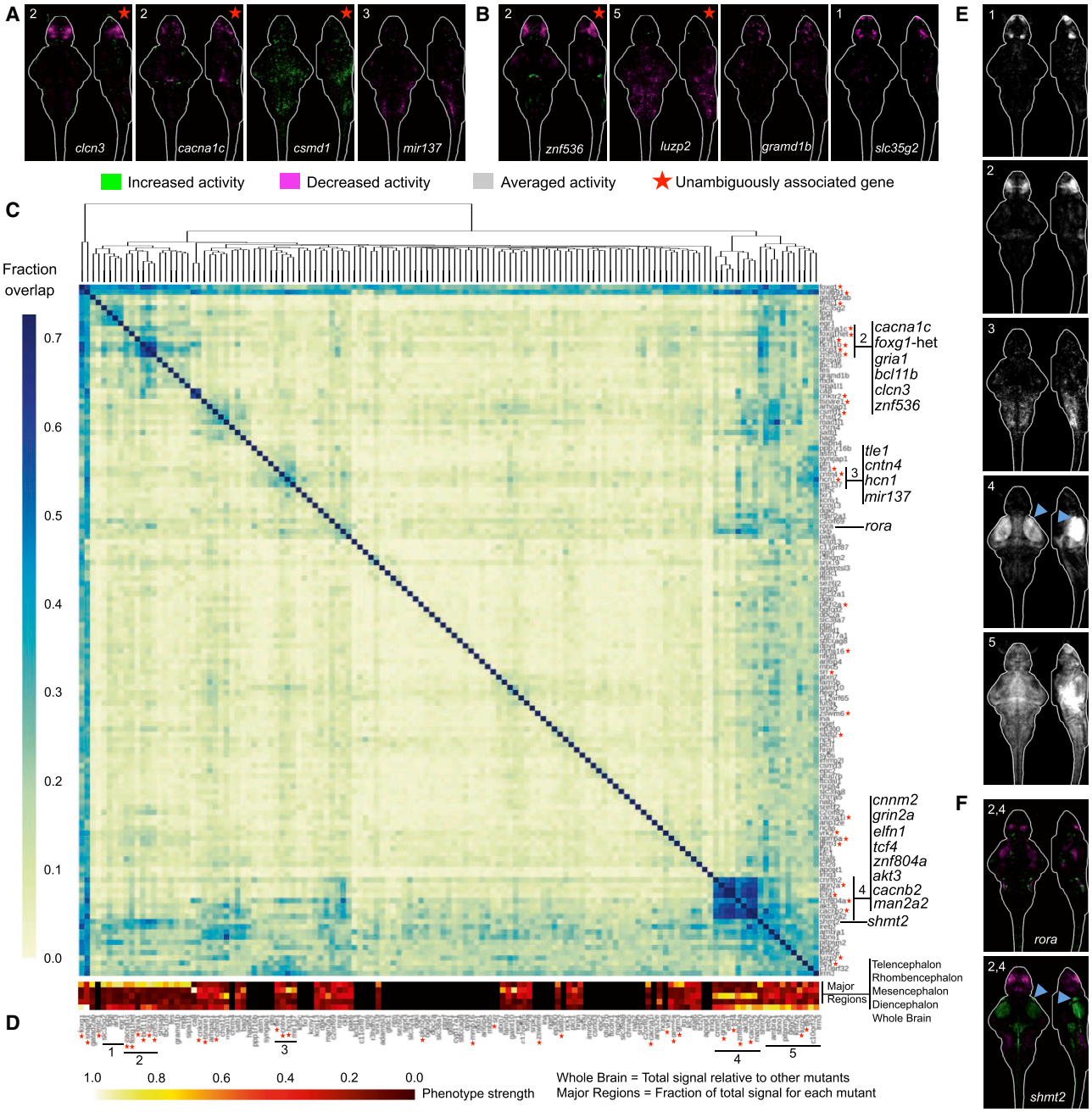

Figure 4. Whole-Brain Activity Phenotypes in Zebrafish Mutants

The number of animals used in all imaging experiments is available in Table S2 (average N is 20 for mutant group, 28 for control group) and on stackjoint.com/zbrain (website naming conventions in STAR Methods). Brain maps were averaged from two independent clutches of larvae if the experiment was repeated and irreproducible signals were eliminated (STAR Methods). The white numbers in the upper right corner of images connect pERK activity maps, both of single genes (panels A and B, and Figure S5) and gene averages (panel E), to the heatmaps and to each other. See also Figure S4. See also Figure S5.

(A) Brain activity phenotypes for genes that have been strongly implicated in schizophrenia by previous studies (Table S1). Sum-of-slices projections of significant differences between mutant and control groups of zebrafish larvae (Randlett et al., 2015). The *cacna1c* mutant phenotype shown is for heterozygous larvae because the homozygous mutant is embryonic lethal (Stainier et al., 1996).

(B) Brain activity phenotypes for four genes that have been minimally studied and have unknown functions.

(C) Percent overlap between mutant brain activity phenotypes was calculated between each image by comparing each brain activity signal to signal in the same location in all other mutant images. These overlaps were then sorted with hierarchical clustering using average linkage. Genes grouped together by this clustering are labeled. The direction of the change in brain activity was disregarded to maximize identification of affected brain regions, and because the direction of the

(legend continued on next page)

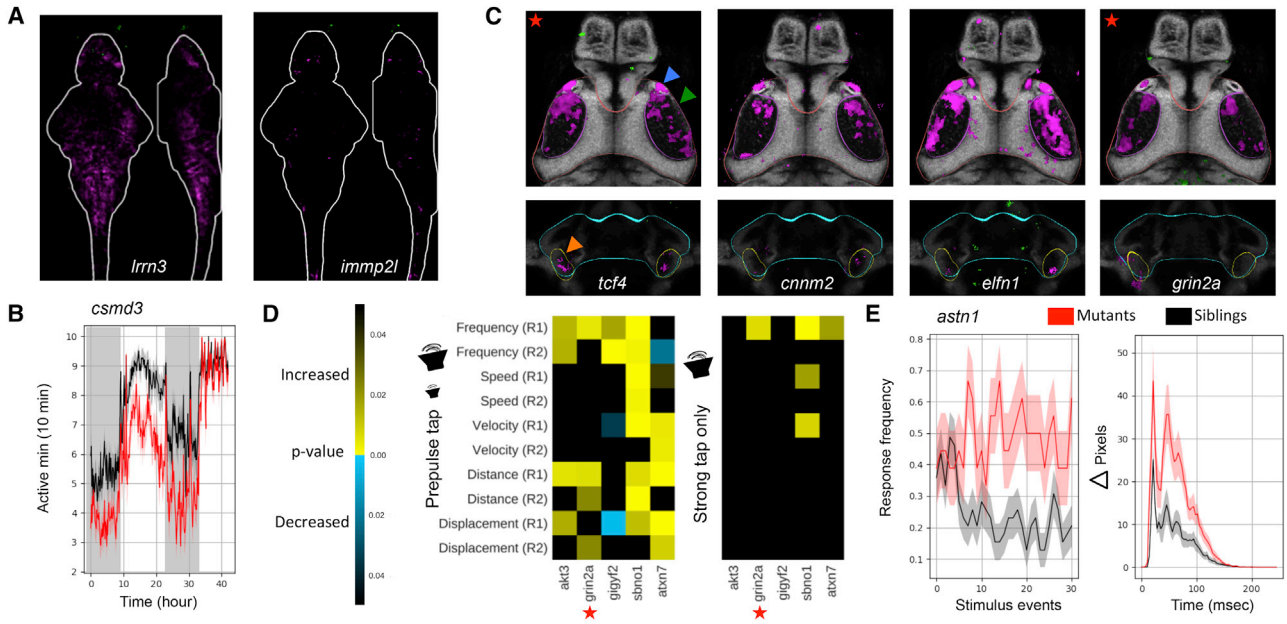

Figure 5. Nominating Candidates in Multi-Gene Loci by Phenotype

The number of animals used in all imaging experiments is available in Table S2 and on stackjoint.com/zbrain.

(A) Brain activity data (sum-of-slices projection) for *lrrn3* and *immp2l* mutants.

(B) Movement frequency for *csmd3* mutants. P value = 0.0001; N = 30 +/- , 29 -/-.

(C) Mutants with tectum (green arrow) and retinal arborization field AF7 (blue arrow, Mesencephalon___Retinal_Arborization_Field_7_AF7 on stackjoint.com/zbrain) phenotypes (representative slices). Mutants with retinal arborization field AF7 signal also display signal changes in the same direction in a small subregion of hypothalamus (orange arrow, Diencephalon___Hypothalamus_Gad1b_Cluster_3_Sparse located within cyan Diencephalon___Intermediate_Hypothalamus; see regions on stackjoint.com/zbrain). See also *kmt2e*, *znf804a*, *cacnb2b*, and *ambra1* (both areas decreased), and *snap91, akt3b*, and *satb1* (both areas increased) on stackjoint.com/zbrain.

(D) Prepulse inhibition phenotypes for five mutants. These mutant phenotypes are specific to the strong prepulse tap (Figure 2J) and do not represent a general increase in tap sensitivity to strong taps (right heatmap). Response features were calculated only on strong tap responses where the weak tap did not elicit movement. See also Figure S3.

(E) Habituation phenotype of *astn1* mutants. Response frequency to tap events occurring every two seconds is shown in left graph, and the magnitude of responses occurring during the habituation paradigm in the right graph. P value for frequency metric = 0.0018; merged p value for the day tap habituation 2 section = 0.015 with 20/47 significant metrics; N = 36 +/- , 18 -/-.

identified over 30 candidates to prioritize for future study (Table S2). For example, two schizophrenia loci (15 and 98) neighbor the genes *immp2l* and *lrrn3*; the *lrrn3* gene is located within the intron of *immp2l*, making it challenging to determine the causal candidate in human genetic studies. Of the two mutated genes, only *lrrn3* had strong brain activity differences (Figure 5A) and numerous behavioral abnormalities (Figure 2G), whereas loss of *immp2l* had minimal effects on brain activity (Figure 5A) and behavior (Figure 2F). Our findings also added credence to candidates suggested by human studies. For example, locus 33 is located in a gene desert, and we mutated three genes (*csmd3*, *sybu*, and *kcnv1*) surrounding the locus. Only one of the three candidates, a second CUB and Sushi domain protein *Csmd3*, had a strong phenotype (Figure 2G, Figure 5B). This gene has a role in dendrite development and has been implicated in autism and epilepsy (Floris et al., 2008; Mizukami et al., 2016).

Clustering mutants by brain activity phenotype (Figure 4C) highlighted potential candidate driver genes in multi-gene loci (Table S2) when one gene in the locus shared phenotypes with unambiguously associated genes. For example, the brain activity of the magnesium transporter *cnnm2* (Arjona et al., 2014) mutant

genetic perturbation in human patients is not clear for most genes. The numbers of image stacks that were compared to calculate significant differences in brain activity for each mutant are available in Table S2.

(D) Contribution of each of the four major brain divisions to the overall brain activity phenotype. The signal in each region was divided by the whole brain signal. Prior to dividing the signal in each region by the total signal, the regions were scaled relative to each other based on their respective sizes (rhombencephalon = *1, diencephalon = *1.76, mesencephalon = *1.42, telencephalon = *4.36). The original whole brain signal was separately scaled across all mutants with a phenotype, indicating the relevance of the signal in each of the regions. Measures below the cutoff for phenotype designation (Figure S1, Figure S2) are displayed in black.

(E). Average signal for mutants with similar brain activity maps. Examples of individual maps that are included in these averages are labeled in panels A and B, as well as in Figure S5. The blue arrow highlights retinal arborization field AF7.

(F) Two mutants with brain activity signals that overlap with both the forebrain (group 2) and the tectum (group 4).

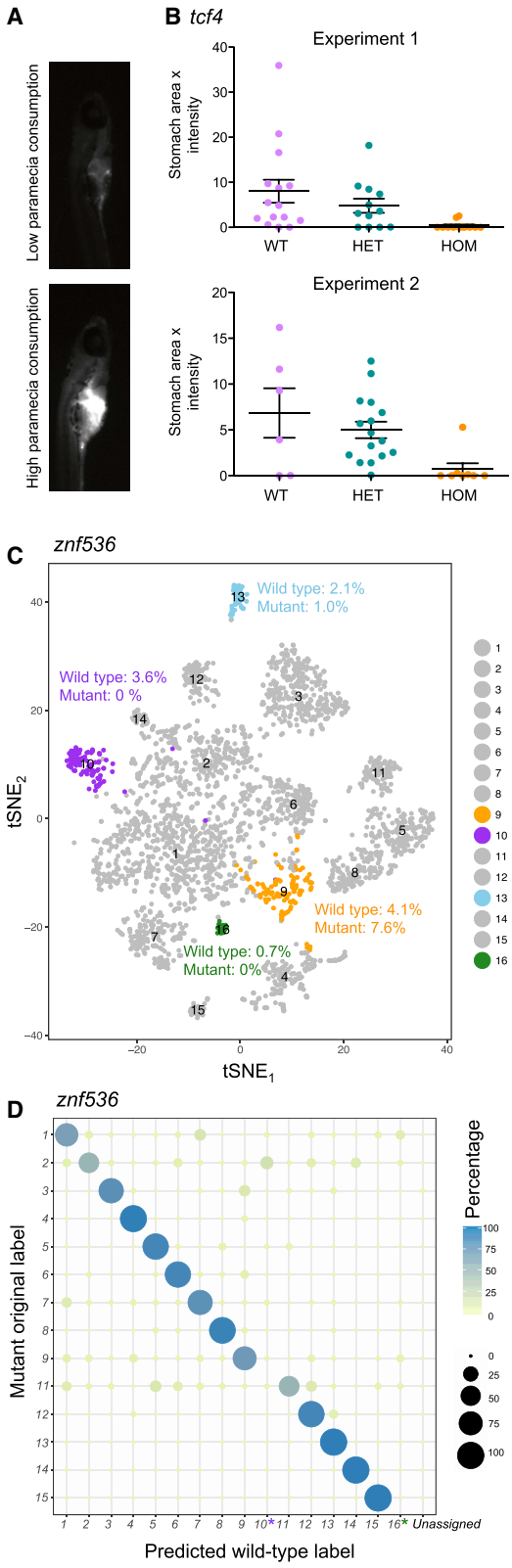

Figure 6. Neurobiological Roles of Top Candidates

(A) Example images of larvae after consuming fluorescently labeled paramecia.

(B) Quantification of feeding behavior in *tcf4* mutants by measurement of paramecia consumed.

(C) T-distributed Stochastic Neighbor Embedding (t-SNE) (Hinton and Maaten, 2008) visualization of wild-type single-cell clusters obtained by clustering of 6 dpf forebrain cells. Clusters with substantial differences in *znf536* mutants are highlighted in orange, purple, and blue. Cluster counts in mutant and wild-type are expressed as percent of the total cell number for each sample. See also Figure S6.

(D) Dotplot (confusion matrix) showing the proportion of cells in the *znf536* mutant forebrain that were classified to wild-type cluster labels. Each mutant forebrain type was assigned to a wild-type cluster label if > 13% of the trees in the Random Forest (RF) model (Breiman, 2001; Pandey et al., 2018) contributed to majority vote.

closely resembled that of mutants for the unambiguously associated transcription factor *tcf4* (Quednow et al., 2014) and the NMDA receptor subunit *grin2a* (Figure 5C). The *cnnm2* locus is ranked 3rd out of the 108 regions and contains more than ten candidates, (Figure 1B), of which we tested five (Table S1, genepile.com/scz_gwas108). The other four mutants from this locus (*arl3*, *cyp17a1*, *c10orf32*, *ina*) did not have phenotypes or did not cluster with unambiguously associated genes (Figure 4C). This result nominates *cnnm2* as a likely driver of this association, highlighting the power of the large-scale approach in defining relevant genes.

Behavioral phenotypes can also help refine multi-gene loci, if behavioral differences have relevance to schizophrenia such as decreased prepulse inhibition and lack of acoustic habituation (Williams et al., 2013). Both of these phenotypes were observed in mutants (Figure 5D, Figure 5E, Figure 2G). Mutants with decreased prepulse inhibition included the translational repressor *gigyf2* (Kryszke et al., 2016; Morita et al., 2012), also linked to autism (Wang et al., 2016), and transcription factor *sbno1*, additionally identified as a possible schizophrenia candidate gene in *de novo* mutation studies (Girard et al., 2011). The gene *astn1*, involved in cerebellar development (Adams et al., 2002), showed a robust decrease in stimulus-driven acoustic habituation (Figure 5E). The fact that similar phenotypes are also observed in some individuals with schizophrenia (Meincke et al., 2004) nominates these genes for stronger consideration as potential drivers of the genetic association of their respective multi-gene loci.

Neurobiological Roles of Top Candidates

Our systematic phenotypic analyses defined top candidates and their neurobiological roles (Table S2). To explore how these datasets can direct follow-up studies, we asked whether mutant brain activity maps could yield hypotheses about potentially affected behaviors. The retinal arborization field AF7 (Figure 4E, label 4; Figure 5C) is known to specifically activate when fish hunt (Semmelhack et al., 2014), and we therefore hypothesized that hunting behavior might be affected in mutants with reduced activity in this area. Indeed, we found that the mutants for the transcription factor *tcf4* (Figure 5C) showed dramatically reduced consumption of live food (Figure 6A, Figure 6B) (Jordi et al., 2015; Shimada et al., 2012). This phenotype was highly specific, as mutants and wild-type displayed similar baseline movement and responses to both light and dark flashes (Figure 2F).

In a second test for the potential of the phenotypic databases in informing follow-up studies, we studied the transcription

factor *znf536* (Figure 1C). Mutants for this gene had volume loss and activity differences in the pallium region of the forebrain (Figure 3C, Figure 4B). To uncover what neuron types might be missing, we profiled the single-cell transcriptomes of dissected mutant and wild-type sibling forebrains (Figure 6C, Figure S6). This comprehensive forebrain map revealed a loss (cluster 10 and cluster 16) and reduction (cluster 12) of cell types (Figure 6C, Figure 6D). All three types uniquely express neuropeptides involved in stress and social behavior: *uts1* in the missing cluster 10, *penkb* in the missing cluster 16, and *tac3b* in the reduced cluster 13. Corresponding with the loss of cell types was an increase in a pool of immature neurons (cluster 9), suggesting a potential developmental mechanism underlying the *znf536* mutant phenotype (Figure 6D, Figure S6). The *tac3b* population is additionally marked by *grm2a* (Figure S6), which is a potential schizophrenia therapeutic target. The identification of these specifically affected types of neurons illustrates the potential of combining our phenotype databases with follow-up analyses such as single-cell RNA sequencing to dissect the biological processes regulated by schizophrenia-associated genes.

DISCUSSION

This study establishes a zebrafish phenotypic atlas for schizophrenia-associated genes and demonstrates the power of large-scale mutant analyses and whole-brain imaging in defining gene function and identifying candidate genes in gene-rich loci (Table S2). Our findings reinforce the contribution of genes and pathways previously implicated in schizophrenia, including glutamatergic neurotransmission (*gria1*, *grin2a*, *elfn1*, *clcn3*), calcium channel function (*cacna1c*, *cacn2b*), neurodevelopment (*bcl11b*, *foxg1, mir137*, *tcf4*, *gpm6a*), and complement regulation (*csmd1*). In addition, we uncover phenotypes for understudied genes, some of which are unambiguously associated (Table S1) with the disorder. Our phenotype atlas also helps address previous biases in gene analyses: major efforts are focused on 10% of human genes, and 27% of human genes have not been studied by a full publication (Stoeger et al., 2018). We provide phenotypic analysis for more than 20 understudied genes with potential disease relevance (Table S1). These candidates include several with previously unknown neurobiological roles (*luzp2*, *gramd1b*, *slc35g2*, *znf536*). Other genes we mutated have undergone some previous characterizations, but our analyses reveal novel phenotypes (*astn1*, *atxn7*, *cnnm2*, *csmd3*, *lrrn3*, *gigyf2*, *kmt2e*, *man2a2*, *tle3*, *vrk2*, *znf804a*). These genes implicate processes such as magnesium transport (Arjona et al., 2014) and translational control (Kryszke et al., 2016) in schizophrenia.

Our systematic approach nominates potential driver genes in multi-gene loci (*cnnm2*, *elfn1*, *shmt2*, *csmd3*, *lrrn3*, *akt3*, *gigyf2*, *rora*, *sbno1*, *atxn7*, *astn1*). This refinement is based on phenotypes shared with unambiguously associated genes and phenotypes relevant to schizophrenia pathology, such as forebrain dysfunction and prepulse inhibition defects. Notably, phenotypic commonalities (Figure 4C, Figure 5C) are detectable not at the molecular level (as in channelopathies) or cellular level (as in ciliopathies) but only at the whole-brain level. For example, 16 seemingly unrelated genes make up the two largest groups of shared phenotypes, affecting activity in the pallium and tectum, respectively (Figure 4). It is tempting to speculate that these molecularly unrelated genes impinge on spatially or temporally overlapping developmental or physiological processes. These genes are excellent choices in gene-rich loci to be the focus of future human genetics studies.

The relevance of our pipeline and dataset extends beyond schizophrenia and zebrafish neurodevelopment. The phenotyping approach introduced in this study can be used to identify candidates and uncover mechanisms for the numerous diseases for which genome-wide association data exists. Many of the genes we tested are involved not only in schizophrenia, but also in autism (Gandal et al., 2018; Grove et al., 2019), epilepsy (Cascella et al., 2009), bipolar disorder (Cross-Disorder Group of the Psychiatric Genomics Consortium, 2013; Gandal et al., 2018), depression (Wray et al., 2018), and sleep disorders (Lane et al., 2017). In addition to shared risk loci, some candidates have been identified by exome studies for these disorders (Dong et al., 2014; Girard et al., 2011; Quednow et al., 2014; Wang et al., 2016). We discovered phenotypes of relevance to autism (Figure 3C). Therefore, our established pipeline and tools can be used to screen genes that are candidates for other disorders, and future mechanistic studies of these genes will provide insights into multiple disorders. Conservation is revealed by the similarities we observe between zebrafish and mammalian phenotypes at the anatomical (*foxg1*, *bcl11b*, *rora*, *akt3*, *slc32a1*) and behavioral (*gpm6*, *akt3*) level, suggesting that large-scale larval zebrafish screens complement studies in mammalian systems.

The mutants described here and available to the community (stackjoint.com, genepile.com) identify among the hundreds of candidate genes at implicated loci (Schizophrenia Working Group of the Psychiatric Genomics Consortium, 2014) some three dozen genes with specific brain phenotypes (Table S2). These genes might be considered stronger candidates to be the focus of detailed mechanistic studies (see Table S2 for genes to prioritize for future studies). The mutants described here can now be analyzed for deficiencies in specific cell types, neuronal connectivity or developmental pathways. For example, using scRNA-seq we discovered that the understudied transcription factor *znf536* has an essential role in development of a small subset of forebrain neurons implicated in stress and social behavior (Figure 6). As these functionalities are disrupted in patients with neuropsychiatric disease, and one of the neuron types is distinctly marked by the therapeutic target *grm2* (Li et al., 2015), this result is a promising lead for future study. Additional phenotypic refinement will include *in vivo* calcium imaging to reveal changes in circuit dynamics in our mutants and determine whether pERK changes in overlapping brain areas are the result of changes to the same neural networks. *In vivo* imaging will also be essential to accurately associate brain activity changes with behavioral phenotypes (Figure S7). Finally, sophisticated behavioral phenotyping tools can now be employed to find subtle defects in our mutant collection. For example, using a feeding assay, we found that *tcf4* is required for food consumption. Future studies will determine whether this phenotype results from a specific AF7-dependent perceptual defect in hunting behavior, decreased appetite or motivation, or an overall reduced visual acuity.

In summary, the phenotype atlas of schizophrenia-associated genes lays the foundation for deciphering the molecular, cellular and physiological pathways underlying neuropsychiatric disease and for high-throughput screens for genetic or small-molecule suppressors of mutant phenotypes (Hoffman et al., 2016; Rennekamp and Peterson, 2015; Rihel et al., 2010).

STAR★METHODS

Detailed methods are provided in the online version of this paper and include the following:

- KEY RESOURCES TABLE
- CONTACT FOR REAGENT AND RESOURCE SHARING
- EXPERIMENTAL MODEL AND SUBJECT DETAILS
  - Zebrafish husbandry
  - Zebrafish model and experimental approach
- METHOD DETAILS
  - Brain activity and morphology
  - Behavior
  - Fluorescent *in situ* hybridization (ISH)
  - Paramecia consumption assay
  - Cell isolation and library preparation for 10X scRNA-seq
- QUANTIFICATION AND STATISTICAL ANALYSIS
  - Brain activity and morphology analysis
  - Image similarity analysis
  - Behavioral Analysis
  - Analysis of single-cell sequencing data
- DATA AND SOFTWARE AVAILABILITY
  - Additional Resources

SUPPLEMENTAL INFORMATION

Supplemental Information can be found online at https://doi.org/10.1016/j.cell.2019.01.048.

ACKNOWLEDGMENTS

We thank the Harvard Center for Biological Imaging for infrastructure and support; fish facility personnel Jessica Miller, Brittany Hughes, Steve Zimmerman and Karen Hurley for supporting this study; Erin Song for assistance with the hunting assay; Stephan Ripke for use of his Manhattan plot image; and William Joo, Philip Abitua, Martin Haesemeyer, Florian Engert, and members of the Schier and Engert labs for helpful feedback; and Akira Sawa and anonymous reviewers for helpful comments on the manuscript. This research was supported by Damon Runyon Cancer Research Foundation (S.B.T.), K99 MH110603 (S.B.T.), Harvard Brain Science Initiative Bipolar Disorder Seed Grant (A.F.S.), Tommy Fuss Center for Neuropsychiatric Disease Seed Grant (A.F.S.), NIH R01 HL109525 and DP1 HD94764 (A.F.S.).

AUTHOR CONTRIBUTIONS

S.B.T. and A.F.S. conceived the project. S.B.T. led all aspects of the research and performed the majority of experimental work and analysis. S.B.T. and A.F.S. wrote the paper, with assistance from E.H.L., Y.W., S.A.M., and S.P., L.M.P., E.H.L., C.S., and J.W.C. contributed to mutant generation and the phenotype screen. E.R.S., J.G., SBT, EHL, S.Z., and L.P. contributed to design and construction of the behavior rigs. S.P. collected and analyzed single-cell sequencing data, with assistance from S.B.T. Y.W. designed and implemented the image clustering and provided input on the behavior analyses. K.J.H. assisted with experiments addressing reviewer comments. O.R. shared phosphorylated-ERK protocols prior to publication and provided helpful feedback, including assistance in establishing the DBM analysis. S.A.M. provided valuable input on schizophrenia genetics. N.S.M. worked with S.B.T. to build stackjoint.com and genepile.com.

DECLARATION OF INTERESTS

The authors declare no competing interests.

Received: June 7, 2018
Revised: October 15, 2018
Accepted: January 27, 2019
Published: March 28, 2019

REFERENCES

Adams, N.C., Tomoda, T., Cooper, M., Dietz, G., and Hatten, M.E. (2002). Mice that lack astrotactin have slowed neuronal migration. Development *129*, 965–972.

Ali, M., Rincón-Arano, H., Zhao, W., Rothbart, S.B., Tong, Q., Parkhurst, S.M., Strahl, B.D., Deng, L.W., Groudine, M., and Kutateladze, T.G. (2013). Molecular basis for chromatin binding and regulation of MLL5. Proc. Natl. Acad. Sci. USA *110*, 11296–11301.

Allou, L., Lambert, L., Amsallem, D., Bieth, E., Edery, P., Destrée, A., Rivier, F., Amor, D., Thompson, E., Nicholl, J., et al. (2012). 14q12 and severe Rett-like phenotypes: new clinical insights and physical mapping of FOXG1-regulatory elements. Eur. J. Hum. Genet. *20*, 1216–1223.

Arjona, F.J., de Baaij, J.H., Schlingmann, K.P., Lameris, A.L., van Wijk, E., Flik, G., Regele, S., Korenke, G.C., Neophytou, B., Rust, S., et al. (2014). CNNM2 mutations cause impaired brain development and seizures in patients with hypomagnesemia. PLoS Genet. *10*, e1004267.

Bamford, R.N., Roessler, E., Burdine, R.D., Saplakoğlu, U., dela Cruz, J., Splitt, M., Goodship, J.A., Towbin, J., Bowers, P., Ferrero, G.B., et al. (2000). Loss-of-function mutations in the EGF-CFC gene CFC1 are associated with human left-right laterality defects. Nat. Genet. *26*, 365–369.

Bergeron, Y., Bureau, G., Laurier-Laurin, M.E., Asselin, E., Massicotte, G., and Cyr, M. (2017). Genetic Deletion of Akt3 Induces an Endophenotype Reminiscent of Psychiatric Manifestations in Mice. Front. Mol. Neurosci. *10*, 102.

Breiman, L. (2001). Random forests. Mach. Learn. *45*, 5–32.

Burgess, H.A., and Granato, M. (2007a). Modulation of locomotor activity in larval zebrafish during light adaptation. J. Exp. Biol. *210*, 2526–2539.

Burgess, H.A., and Granato, M. (2007b). Sensorimotor gating in larval zebrafish. J. Neurosci. *27*, 4984–4994.

Cachero, S., Ostrovsky, A.D., Yu, J.Y., Dickson, B.J., and Jefferis, G.S. (2010). Sexual dimorphism in the fly brain. Curr. Biol. *20*, 1589–1601.

Cascella, N.G., Schretlen, D.J., and Sawa, A. (2009). Schizophrenia and epilepsy: is there a shared susceptibility? Neurosci. Res. *63*, 227–235.

Chen, B., Wang, S.S., Hattox, A.M., Rayburn, H., Nelson, S.B., and McConnell, S.K. (2008). The Fezf2-Ctip2 genetic pathway regulates the fate choice of subcortical projection neurons in the developing cerebral cortex. Proc. Natl. Acad. Sci. USA *105*, 11382–11387.

Conklin, E.E., Lee, K.L., Schlabach, S.A., and Woods, I.G. (2015). VideoHacking: Automated Tracking and Quantification of Locomotor Behavior with Open Source Software and Off-the-Shelf Video Equipment. J. Undergrad. Neurosci. Educ. *13*, A120–A125.

Cross-Disorder Group of the Psychiatric Genomics Consortium (2013). Identification of risk loci with shared effects on five major psychiatric disorders: a genome-wide analysis. Lancet *381*, 1371–1379.

Dong, S., Walker, M.F., Carriero, N.J., DiCola, M., Willsey, A.J., Ye, A.Y., Waqar, Z., Gonzalez, L.E., Overton, J.D., Frahm, S., et al. (2014). De novo insertions and deletions of predominantly paternal origin are associated with autism spectrum disorder. Cell Rep. *9*, 16–23.

Driever, W., Solnica-Krezel, L., Schier, A.F., Neuhauss, S.C., Malicki, J., Stemple, D.L., Stainier, D.Y., Zwartkruis, F., Abdelilah, S., Rangini, Z., et al. (1996).

A genetic screen for mutations affecting embryogenesis in zebrafish. Development *123*, 37–46.

Eagleson, K.L., Schlueter McFadyen-Ketchum, L.J., Ahrens, E.T., Mills, P.H., Does, M.D., Nickols, J., and Levitt, P. (2007). Disruption of Foxg1 expression by knock-in of cre recombinase: effects on the development of the mouse telencephalon. Neuroscience *148*, 385–399.

Easton, R.M., Cho, H., Roovers, K., Shineman, D.W., Mizrahi, M., Forman, M.S., Lee, V.M., Szabolcs, M., de Jong, R., Oltersdorf, T., et al. (2005). Role for Akt3/protein kinase Bgamma in attainment of normal brain size. Mol. Cell. Biol. *25*, 1869–1878.

El-Kordi, A., Kästner, A., Grube, S., Klugmann, M., Begemann, M., Sperling, S., Hammerschmidt, K., Hammer, C., Stepniak, B., Patzig, J., et al. (2013). A single gene defect causing claustrophobia. Transl. Psychiatry *3*, e254.

Escamilla, C.O., Filonova, I., Walker, A.K., Xuan, Z.X., Holehonnur, R., Espinosa, F., Liu, S., Thyme, S.B., López-García, I.A., Mendoza, D.B., et al. (2017). Kctd13 deletion reduces synaptic transmission via increased RhoA. Nature *551*, 227–231.

Floris, C., Rassu, S., Boccone, L., Gasperini, D., Cao, A., and Crisponi, L. (2008). Two patients with balanced translocations and autistic disorder: CSMD3 as a candidate gene for autism found in their common 8q23 breakpoint area. Eur. J. Hum. Genet. *16*, 696–704.

Fromer, M., Roussos, P., Sieberts, S.K., Johnson, J.S., Kavanagh, D.H., Perumal, T.M., Ruderfer, D.M., Oh, E.C., Topol, A., Shah, H.R., et al. (2016). Gene expression elucidates functional impact of polygenic risk for schizophrenia. Nat. Neurosci. *19*, 1442–1453.

Gandal, M.J., Haney, J.R., Parikshak, N.N., Leppa, V., Ramaswami, G., Hartl, C., Schork, A.J., Appadurai, V., Buil, A., Werge, T.M., et al.; CommonMind Consortium; PsychENCODE Consortium; iPSYCH-BROAD Working Group (2018). Shared molecular neuropathology across major psychiatric disorders parallels polygenic overlap. Science *359*, 693–697.

Genovese, G., Fromer, M., Stahl, E.A., Ruderfer, D.M., Chambert, K., Landén, M., Moran, J.L., Purcell, S.M., Sklar, P., Sullivan, P.F., et al. (2016). Increased burden of ultra-rare protein-altering variants among 4,877 individuals with schizophrenia. Nat. Neurosci. *19*, 1433–1441.

Girard, S.L., Gauthier, J., Noreau, A., Xiong, L., Zhou, S., Jouan, L., Dionne-Laporte, A., Spiegelman, D., Henrion, E., Diallo, O., et al. (2011). Increased exonic de novo mutation rate in individuals with schizophrenia. Nat. Genet. *43*, 860–863.

Grove, J., Ripke, S., Als, T.D., Mattheisen, M., Walters, R., Won, H., Pallesen, J., Agerbo, E., Andreassen, O.A., Anney, R., et al. (2019). Common risk variants identified in autism spectrum disorder. Nat. Genet. *51*, 431–444.

Guella, I., Pistocchi, A., Asselta, R., Rimoldi, V., Ghilardi, A., Sironi, F., Trotta, L., Primignani, P., Zini, M., Zecchinelli, A., et al. (2011). Mutational screening and zebrafish functional analysis of GIGYF2 as a Parkinson-disease gene. Neurobiol. Aging *32*, 1994–2005.

Haesemeyer, M., and Schier, A.F. (2015). The study of psychiatric disease genes and drugs in zebrafish. Curr. Opin. Neurobiol. *30*, 122–130.

Haffter, P., Granato, M., Brand, M., Mullins, M.C., Hammerschmidt, M., Kane, D.A., Odenthal, J., van Eeden, F.J., Jiang, Y.J., Heisenberg, C.P., et al. (1996). The identification of genes with unique and essential functions in the development of the zebrafish, Danio rerio. Development *123*, 1–36.

Heyes, S., Pratt, W.S., Rees, E., Dahimene, S., Ferron, L., Owen, M.J., and Dolphin, A.C. (2015). Genetic disruption of voltage-gated calcium channels in psychiatric and neurological disorders. Prog. Neurobiol. *134*, 36–54.

Hinton, G., and Maaten, L.d. (2008). Visualizing Data using t-SNE. J. Mach. Learn. Res. *9*, 2579–2605.

Hoffman, E.J., Turner, K.J., Fernandez, J.M., Cifuentes, D., Ghosh, M., Ijaz, S., Jain, R.A., Kubo, F., Bill, B.R., Baier, H., et al. (2016). Estrogens Suppress a Behavioral Phenotype in Zebrafish Mutants of the Autism Risk Gene, CNTNAP2. Neuron *89*, 725–733.

Jefferis, G.S., Potter, C.J., Chan, A.M., Marin, E.C., Rohlfing, T., Maurer, C.R., Jr., and Luo, L. (2007). Comprehensive maps of Drosophila higher olfactory centers: spatially segregated fruit and pheromone representation. Cell *128*, 1187–1203.

Jordi, J., Guggiana-Nilo, D., Soucy, E., Song, E.Y., Lei Wee, C., and Engert, F. (2015). A high-throughput assay for quantifying appetite and digestive dynamics. Am. J. Physiol. Regul. Integr. Comp. Physiol. *309*, R345–R357.

Kettleborough, R.N., Busch-Nentwich, E.M., Harvey, S.A., Dooley, C.M., de Bruijn, E., van Eeden, F., Sealy, I., White, R.J., Herd, C., Nijman, I.J., et al. (2013). A systematic genome-wide analysis of zebrafish protein-coding gene function. Nature *496*, 494–497.

Kryszke, M.H., Adjeriou, B., Liang, F., Chen, H., and Dautry, F. (2016). Post-transcriptional gene silencing activity of human GIGYF2. Biochem. Biophys. Res. Commun. *475*, 289–294.

Lane, J.M., Liang, J., Vlasac, I., Anderson, S.G., Bechtold, D.A., Bowden, J., Emsley, R., Gill, S., Little, M.A., Luik, A.I., et al. (2017). Genome-wide association analyses of sleep disturbance traits identify new loci and highlight shared genetics with neuropsychiatric and metabolic traits. Nat. Genet. *49*, 274–281.

Lein, E.S., Hawrylycz, M.J., Ao, N., Ayres, M., Bensinger, A., Bernard, A., Boe, A.F., Boguski, M.S., Brockway, K.S., Byrnes, E.J., et al. (2007). Genome-wide atlas of gene expression in the adult mouse brain. Nature *445*, 168–176.

Li, M.L., Hu, X.Q., Li, F., and Gao, W.J. (2015). Perspectives on the mGluR2/3 agonists as a therapeutic target for schizophrenia: Still promising or a dead end? Prog. Neuropsychopharmacol. Biol. Psychiatry *60*, 66–76.

Mariani, J., Coppola, G., Zhang, P., Abyzov, A., Provini, L., Tomasini, L., Amenduni, M., Szekely, A., Palejev, D., Wilson, M., et al. (2015). FOXG1-Dependent Dysregulation of GABA/Glutamate Neuron Differentiation in Autism Spectrum Disorders. Cell *162*, 375–390.

Meincke, U., Light, G.A., Geyer, M.A., Braff, D.L., and Gouzoulis-Mayfrank, E. (2004). Sensitization and habituation of the acoustic startle reflex in patients with schizophrenia. Psychiatry Res. *126*, 51–61.

Mizukami, T., Kohno, T., and Hattori, M. (2016). CUB and Sushi multiple domains 3 regulates dendrite development. Neurosci. Res. *110*, 11–17.

Morita, M., Ler, L.W., Fabian, M.R., Siddiqui, N., Mullin, M., Henderson, V.C., Alain, T., Fonseca, B.D., Karashchuk, G., Bennett, C.F., et al. (2012). A novel 4EHP-GIGYF2 translational repressor complex is essential for mammalian development. Mol. Cell. Biol. *32*, 3585–3593.

Pandey, S., Shekhar, K., Regev, A., and Schier, A.F. (2018). Comprehensive Identification and Spatial Mapping of Habenular Neuronal Types Using Single-Cell RNA-Seq. Curr. Biol. *28*, 1052–1065 e1057.

Quednow, B.B., Brzózka, M.M., and Rossner, M.J. (2014). Transcription factor 4 (TCF4) and schizophrenia: integrating the animal and the human perspective. Cell. Mol. Life Sci. *71*, 2815–2835.

Randlett, O., Wee, C.L., Naumann, E.A., Nnaemeka, O., Schoppik, D., Fitzgerald, J.E., Portugues, R., Lacoste, A.M., Riegler, C., Engert, F., and Schier, A.F. (2015). Whole-brain activity mapping onto a zebrafish brain atlas. Nat. Methods *12*, 1039–1046.

Redcay, E., and Courchesne, E. (2005). When is the brain enlarged in autism? A meta-analysis of all brain size reports. Biol. Psychiatry *58*, 1–9.

Rennekamp, A.J., and Peterson, R.T. (2015). 15 years of zebrafish chemical screening. Curr. Opin. Chem. Biol. *24*, 58–70.

Rihel, J., Prober, D.A., Arvanites, A., Lam, K., Zimmerman, S., Jang, S., Haggarty, S.J., Kokel, D., Rubin, L.L., Peterson, R.T., and Schier, A.F. (2010). Zebrafish behavioral profiling links drugs to biological targets and rest/wake regulation. Science *327*, 348–351.

Rohlfing, T., and Maurer, C.R., Jr. (2003). Nonrigid image registration in shared-memory multiprocessor environments with application to brains, breasts, and bees. IEEE Trans. Inf. Technol. Biomed. *7*, 16–25.

Roth, M., Bonev, B., Lindsay, J., Lea, R., Panagiotaki, N., Houart, C., and Papalopulu, N. (2010). FoxG1 and TLE2 act cooperatively to regulate ventral telencephalon formation. Development *137*, 1553–1562.

Satija, R., Farrell, J.A., Gennert, D., Schier, A.F., and Regev, A. (2015). Spatial reconstruction of single-cell gene expression data. Nat. Biotechnol. *33*, 495–502.

Schizophrenia Working Group of the Psychiatric Genomics Consortium (2014). Biological insights from 108 schizophrenia-associated genetic loci. Nature *511*, 421–427.

Sekar, A., Bialas, A.R., de Rivera, H., Davis, A., Hammond, T.R., Kamitaki, N., Tooley, K., Presumey, J., Baum, M., Van Doren, V., et al.; Schizophrenia Working Group of the Psychiatric Genomics Consortium (2016). Schizophrenia risk from complex variation of complement component 4. Nature *530*, 177–183.

Semmelhack, J.L., Donovan, J.C., Thiele, T.R., Kuehn, E., Laurell, E., and Baier, H. (2014). A dedicated visual pathway for prey detection in larval zebrafish. eLife *3*, 3.

Shimada, Y., Hirano, M., Nishimura, Y., and Tanaka, T. (2012). A high-throughput fluorescence-based assay system for appetite-regulating gene and drug screening. PLoS ONE *7*, e52549.

Sidman, R.L., Lane, P.W., and Dickie, M.M. (1962). Staggerer, a new mutation in the mouse affecting the cerebellum. Science *137*, 610–612.

Söllner, C., Rauch, G.J., Siemens, J., Geisler, R., Schuster, S.C., Müller, U., and Nicolson, T.; Tübingen 2000 Screen Consortium (2004). Mutations in cadherin 23 affect tip links in zebrafish sensory hair cells. Nature *428*, 955–959.

Stainier, D.Y., Fouquet, B., Chen, J.N., Warren, K.S., Weinstein, B.M., Meiler, S.E., Mohideen, M.A., Neuhauss, S.C., Solnica-Krezel, L., Schier, A.F., et al. (1996). Mutations affecting the formation and function of the cardiovascular system in the zebrafish embryo. Development *123*, 285–292.

Stoeger, T., Gerlach, M., Morimoto, R.I., and Nunes Amaral, L.A. (2018). Large-scale investigation of the reasons why potentially important genes are ignored. PLoS Biol. *16*, e2006643.

Wang, T., Guo, H., Xiong, B., Stessman, H.A., Wu, H., Coe, B.P., Turner, T.N., Liu, Y., Zhao, W., Hoekzema, K., et al. (2016). De novo genic mutations among a Chinese autism spectrum disorder cohort. Nat. Commun. *7*, 13316.

Williams, L.E., Blackford, J.U., Luksik, A., Gauthier, I., and Heckers, S. (2013). Reduced habituation in patients with schizophrenia. Schizophr. Res. *151*, 124–132.

Wilson, S.W., Brand, M., and Eisen, J.S. (2002). Patterning the zebrafish central nervous system. Results Probl. Cell Differ. *40*, 181–215.

Wojcik, S.M., Katsurabayashi, S., Guillemin, I., Friauf, E., Rosenmund, C., Brose, N., and Rhee, J.S. (2006). A shared vesicular carrier allows synaptic corelease of GABA and glycine. Neuron *50*, 575–587.

Wolman, M.A., Jain, R.A., Liss, L., and Granato, M. (2011). Chemical modulation of memory formation in larval zebrafish. Proc. Natl. Acad. Sci. USA *108*, 15468–15473.

Won, H., de la Torre-Ubieta, L., Stein, J.L., Parikshak, N.N., Huang, J., Opland, C.K., Gandal, M.J., Sutton, G.J., Hormozdiari, F., Lu, D., et al. (2016). Chromosome conformation elucidates regulatory relationships in developing human brain. Nature *538*, 523–527.

Wray, N.R., Ripke, S., Mattheisen, M., Trzaskowski, M., Byrne, E.M., Abdellaoui, A., Adams, M.J., Agerbo, E., Air, T.M., Andlauer, T.M.F., et al.; eQTLGen; 23andMe; Major Depressive Disorder Working Group of the Psychiatric Genomics Consortium (2018). Genome-wide association analyses identify 44 risk variants and refine the genetic architecture of major depression. Nat. Genet. *50*, 668–681.

STAR★METHODS

KEY RESOURCES TABLE

REAGENT or RESOURCE	SOURCE	IDENTIFIER
Antibodies		
Anti-phosphorylated-Erk	Cell Signaling	CAT#4370; RRID:AB_2315112
Anti-total-Erk	Cell Signaling	CAT#4696; RRID:AB_390780
Anti-DIG POD	Roche	CAT#11207733910; RRID:AB_514500
Chemicals, Peptides, and Recombinant Proteins		
Cy3 tyramide reagent	Perkin Elmer	CAT#NEL744991KT
Earle's Balanced Salt Solution	Worthington	CAT#LS003126
Papain	Worthington	CAT#LS003126
Neurobasal	ThermoFisher Scientific	CAT#21103049
B27	ThermoFisher Scientific	CAT#A8806
BSA	NEB	CAT#B9000S
TCL Buffer	QIAGEN	CAT#1031576
1% 2-mercaptoethanol	Sigma	CAT#63689
Ovomucoid solution	Worthington	CAT#LS003087
Paraformaldehyde	Supplier Polysciences, Inc.	CAT#04018-1
DiD' dye	ThermoFisher Scientific	CAT# D7757
Deposited Data		
Raw data files for single-cell RNA-sequencing	NCBI Gene Expression Omnibus	GSE115427
RNA-FISH Stacks	This paper: stackjoint.com/basic	Search for Tag: "Thyme, 2018"
Brain activity maps	This paper: stackjoint.com/zbrain	Search for Tag: "Thyme, 2018"
Behavior data	Zenodo	https://doi.org/10.5281/zenodo.2522485
Experimental Models: Organisms/Strain		
Zebrafish: 132 mutant lines	This paper	genepile.com/scz_gwas108
Critical Commercial Assays		
10X reagents	10X Genomics	Chromium Single Cell 3′v2 Reagent Kits
Software		
stackjoint.com, a community resource, where users can upload their own data, explore it, and share it	This paper	stackjoint.com
Labview code for tracking larvae and generating high-speed movies	This paper	https://github.com/cbs-ntcore/Schier-Lab
All analysis code for behavior and imaging data	This paper	https://github.com/sthyme/ZFSchizophrenia
MapMAPPing	(Randlett et al., 2015)	https://github.com/owenrandlett/Z-Brain
MATLAB	MathWorks	https://www.mathworks.com/products/matlab.html
CMTK	(Jefferis et al., 2007; Rohlfing and Maurer, 2003)	https://www.nitrc.org/projects/cmtk
ImageJ	NIH	https://imagej.nih.gov/ij/index.html
Cellranger	10X Genomics	https://support.10xgenomics.com/single-cell-gene-expression/software/pipelines/latest/what-is-cell-ranger
PCA, clustering and differential expression	(Satija et al., 2015)	R library Seurat
t-distributed Stochastic Neighbor Embedding	(Hinton and Maaten, 2008)	https://lvdmaaten.github.io/tsne/

(*Continued on next page*)

Continued		
REAGENT or RESOURCE	SOURCE	IDENTIFIER
Random Forest Classification	(Breiman, 2001; Pandey et al., 2018)	R package Random Forest
UMI based variable gene selection	(Pandey et al., 2018)	N/A
Other		
Resource website	This paper	stackjoint.com
Resource website	This paper	genepile.com
96-well square 0.7 mL plates	E&K Scientific	Cat#2074
Optical adhesive films	ThermoFisher Scientific	Cat#4311971
Grasshopper3 camera	FLIR	Cat#GS3-U3-23S6M-C

CONTACT FOR REAGENT AND RESOURCE SHARING

Further information and requests for resources and reagents should be directed to and will be fulfilled by the Lead Contact, Summer B. Thyme (sthyme@gmail.com).

EXPERIMENTAL MODEL AND SUBJECT DETAILS

Zebrafish husbandry

All protocols and procedures involving zebrafish were approved by the Harvard University/Faculty of Arts & Sciences Standing Committee on the Use of Animals in Research and Teaching (IACUC; Protocol #25-08). Mutants were generated by simultaneous injection of one to four guide RNAs (gRNAs), and approximately 0.5 nL of 50 μM Cas9 protein into EK/*nacre* (*mitfa*$^{-/-}$) embryos. Sequences of all gRNAs and resulting mutations are available on genepile.com. The resulting mosaic adults with a germline mutagenic deletion were crossed to either EK or *nacre* and the offspring were mated to each other to generate homozygous mutants. If the human gene of interest was duplicated in zebrafish, homozygous mutations were generated for both orthologs. Tests of duplicated genes were most often completed with double homozygous (-/-:-/-) compared to +/-;+/-, +/-;-/-, and -/-;+/- siblings (exact comparisons described in Table S2). Including orthologs, we mutated 165 individual zebrafish genes corresponding to 132 human genes. All larvae were genotyped to generate lines and for all phenotypic characterizations. Zebrafish were raised at 28.5°C on a 14/10 hour light/dark cycle. Behavioral experiments were conducted on the same cycle and at the same temperature. Fish used for all assays were grown in 150 mm Petri dishes in fish water containing methylene blue, at a density of less than 160 larvae per dish, and debris was removed twice prior to 4 dpf. All assays were conducted on larvae from 4-6 dpf. At this developmental stage the sex of the organism is not yet determined.

Zebrafish model and experimental approach

Schizophrenia is a human disease typically associated with SNPs in regulatory regions, not with deletion alleles in precisely defined protein-coding genes. Our goal was not to precisely model human alleles and symptoms in larval zebrafish but was instead to define the function of genes in and near schizophrenia-associated loci. Given the modest penetrance of each schizophrenia risk allele in isolation and their lack of non-coding conservation even between human and other mammalian genomes, it would be naive and likely technically impossible to create animal lines with human schizophrenia-associated SNPs. We established this zebrafish-based pipeline in order to perform rapid *in vivo* analysis, leveraging the high-throughput advantages of this small vertebrate, and gain insight into neurobiological mechanisms involving putative schizophrenia-associated genes.

Both zebrafish models and knockout studies have provided insight into understanding human disease, including psychiatric disease. Homozygous knockouts are the basis for the entire mouse phenotyping consortium, and there are numerous cases where psychiatric disease research has specifically benefited from loss-of-function studies (Escamilla et al., 2017; Sekar et al., 2016). Studies of gene knockouts in zebrafish have established neurodevelopmental functions of the autism-linked gene *cntnap2* (Hoffman et al., 2016), uncovered the mechanism underlying a human deafness syndrome (Söllner et al., 2004), and assisted in the discovery of genes underlying human laterality defects (Bamford et al., 2000). In addition, human exome studies of multiple neurological diseases (intellectual disability, schizophrenia, epilepsy, bipolar disorder, and autism) have identified truncating loss-of-function mutations in many of the candidates we have tested (Table S1). These complementary genetic findings underscore the clear role of these genes in pathways underlying human neuropsychiatric phenomena. For example, loss of CNNM2 is linked to human intellectual disability (Arjona et al., 2014), and a truncating allele was found in schizophrenia patients by a large-scale exome analysis (Genovese et al., 2016) (see Table S3 in Genovese et al.).

METHOD DETAILS

Brain activity and morphology

Phosphorylated-ERK antibody staining was conducted as previously described (Randlett et al., 2015). The protein ERK is excluded from the nucleus, and is phosphorylated in zebrafish neurons 10 s after calcium signaling (Randlett et al., 2015). Phosphorylated ERK can then translocate to the nucleus. Differences in ERK phosphorylation in neuropil in brain activity mapping could be due to signaling that will result in nuclear translocation or to signaling with a terminal-specific function. Larvae were fed paramecia in the morning of 5 dpf. On 6 dpf they were maintained in a quiet environment and fixed in the mid-afternoon in 4% paraformaldehyde (PFA) (Supplier Polysciences) diluted in 1X Phosphate Buffered Saline with 0.25% Triton (PBST). To ensure rapid fixation in less than 10 s after neuronal stimulation, larvae were poured into a mesh sieve and immediately submerged in fix. After overnight fixation, larvae were washed three times for 15 min each in PBST. Pigment on larvae was bleached with a 1% H_2O_2/3% KOH solution, followed by three 15-min washes in PBST. Larvae were then incubated at 70°C for 20 min in 150 mM TrisHCl pH 9.0, to retrieve antigens, followed by two five-minute washes in PBST. Permeabilization of tissue was conducted by incubation in 0.05% Trypsin-EDTA on ice for 45 min. After three 15-min washes and blocking for one hour (PBST with 2% normal goat serum (NGS), 1% bovine serum albumin (BSA), and 1% dimethyl sulfoxide (DMSO)), primary antibodies were diluted in blocking solution and incubated overnight. The phosphorylated ERK antibody (Cell Signaling, #4370) and total ERK antibody (Cell Signaling, #4696) were diluted both 1:500. The following day larvae were rinsed three times for 15 min each with PBST, and alexa-fluorophore conjugated secondary antibodies (Life Technologies) were diluted 1:500 in blocking solution for a second overnight incubation. Following three 15-min PBST washes, larvae were mounted in 2% low-melting agarose in 1X PBS. Images were collected using either Zeiss LSM 780 or 880 upright confocal microscopes with a 20X/1.0 NA water-dipping objective. Of the 132 mutants, 78 were independently repeated to confirm results (Table S2, stackjoint.com/zbrain). Larvae were removed from the agarose and genotyped after imaging.

Behavior

The majority of assays were conducted with between 24 and 96 larvae in a multi-well plate (exact Ns in Table S2). Fish were transferred to 96-well square 0.7 mL plates (E&K Scientific) on the afternoon of 4 dpf. Plates were filled with standard fish water containing methylene blue, transferred to ice until locomotion ceased, and sealed with optical adhesive films (ThermoFisher Scientific). Experiments were conducted at approximately 28°C. Larval locations were monitored at approximately 30 frames-per-second (fps) with 1088 × 660-pixel resolution during the entire time course using a Grasshopper3 camera (FLIR). To monitor stimulus responses, the camera generated one-second long movies at 285 fps. Tap stimuli were delivered by computer-controlled increases in voltage to a solenoid attached to the apparatus. Tap strengths for weak and strong taps were determined based on percent of larvae responding. The strong was set as high as possible, with almost 100% of the fish responding if they had not habituated to the stimulus. The weak tap was set so that less than 10% of the larvae responded. We repeated behavioral assessments for 73 of the mutants, including 46 mutants of the 49 designated as having a behavioral phenotype (Figure 2G, Figure S1, Figure S2, Table S2). The genes *rora*, *dgkz*, and *pitpnm2* were designated as having a phenotype but were not repeated. The protocol lasted two days and was analyzed as 14 time windows, some of which contained stimuli that are detailed as follows:

Time windows

1) Night 1, 11:59 pm – 8:59 am, 9 hours, no events and lights were off.

(2) Morning transition 1, 9:00 am – 9:10 am, 10 minutes, lights turned on to a low level at 9:00 am.

(3) Morning light flash, 9:10 am – 11:15 am, 125 minutes, twenty 1-second long light flashes with 1-minute spacing starting at 9:11 am.

(4) Day baseline, 11:15 am – 2:00 pm, 165 minutes, no events and lights were at a standard intermediate level.

(5) Day taps, 2:00 pm – 7:22 pm, prepulse inhibition and short-term tap habituation, 5 hours and 22 minutes. Randomly intermixed strong, weak, and prepulse taps occurred from 2:00 pm – 5:00 pm, with spacing of 30 seconds. Three blocks of tap habituation occurred from 5:30 pm – 7:07 pm. Each block consists of 10 strong taps with spacing of 30 seconds (pre-habituation), followed by a 10-minute break and then 33 strong habituating taps with 2 second spacing. Of the 36 taps, numbers 4, 19, 36 are high-speed (computer cannot process high-speed movies every 2 seconds) and used to calculate habituation phenotypes This habituation section was followed by a 3-minute break, and then 10 taps separated by 30 seconds. Then the second habituation block began (taps every 2 seconds), and the cycle was repeated once more for the 3rd block.

(6) Evening, 7:22 pm – 10:59 pm, 217 minutes, no events and lights were at standard intermediate level.

(7) Night transition, 11:00 pm – 11:10 pm, 10 minutes, lights turned off at 11:00 pm.

(8) Night 2, 11:10 pm – 1:00 am, 110 minutes, no events and lights were off.

(9) Night stimulation, 1:00 am – 7:00 am, including tap habituation, prepulse tests, tap response threshold tests, and light flash stimulation, 6 hours. This window included 1 hour of random strong, weak, and prepulse (weak, followed by strong 300 milliseconds later) taps, followed by one habituation block, followed by twenty light flashes.

(10) Night 2b, 7:00 am – 8:59 am, second section, 119 minutes, no events and lights were off.

(11) Morning transition 2, 9:00 am – 9:10 am, 10 minutes, lights turned to standard intermediate level at 9:00 am.

(12) Morning 2, 9:10 am – 10:00 am, 50 minutes, no events and lights were at standard intermediate level.

(13) Dark flashes, 10:00 am – 5:00 pm, 7 hours, four 1-hour blocks of 1-second long dark flashes with 1 minute spacing. Each block is spaced by 1-hour of rest. The first 10 and last 10 flashes of each of the four blocks are recorded at high-speed and analyzed to determine dark flash responsiveness over the course the experiment (flash responses 11-50 are not analyzed).

(14) Heat stressor, after 5:00 pm, >70 minutes, manually turned on water heater and system took 10-15 minutes to reach a 10°C increase that was maintained for approximately 1 hour.

Fluorescent *in situ* hybridization (ISH)

Fluorescent RNA ISHs (Figure S5) were performed as previously described (Pandey et al., 2018) using 6 dpf *mitfa*−/− larvae. To generate probes, gene fragments were amplified from with Phusion polymerase (New England Biolabs, M0530L). Sequences for data shown in Figure S5 are available on genepile.com. The fragments were cloned, and resulting plasmids were linearized with restriction digestion and purified using a PCR clean up kit (Omega Cycle Pure Kit). Digoxigenin-labeled RNA probes were generated using the RNA labeling kit (Roche) and purified using Total RNA clean up kit (Omega, R6834). The quality of the probes was confirmed on an agarose gel and concentration was quantified using Nanodrop. The final product was diluted to 50 ng/μL in Hybridization Mix (HM+) buffer (50% formamide, 5X Saline Sodium Citrate (SSC) buffer, 0.1% Tween 20, 5 50 μg/mL heparin, mg/mL torula RNA).

Larvae were fixed in 4% PFA diluted in PBS at 4°C overnight, and subsequently rinsed three times in *in situ* PBST (PBS with 0.1% Tween 20). Larvae were then dehydrated with increasing methanol (MEOH) concentration diluted in PBST, incubating for 10 min each in 25%, 50%, 75%, 100%, and 100% MEOH. Following at least one overnight at −20°C, larvae were rehydrated with decreasing concentrations of MEOH diluted in PBST (10 min incubation, 75%, 50%, 25%, 0% four times). Larvae were then incubated in Proteinase K for 1 hour at a concentration of 10 μg/mL and the reaction was halted by incubating in 4% PFA for 20 min. Larvae were pre-hybridized in HM+ buffer for 2 hours at 65°C. Probes, normalized to 3.33 ng/μL, were denatured at 70°C for 10 min before hybridization, which was conducted overnight in HM+ buffer at 65°C. Larvae were washed the next day at 65°C first for 20 min each in HM+ buffer, 75% formamide diluted in 25% SSCT buffer (2X SSC with 0.1% Tween 20), 50% formamide with 50% SSCT, 25% formamide with 75% SSCT, 100% SSCT, 100% SSCT, and then three times for 30 min in 0.2X SSCT and twice in room temperature for 10 min in TNT (100mM Tris-HCl, pH 7.5, 150mM NaCl, 0.5% Tween 20). Blocking for a minimum of 1 hour (TNTB: 1% blocking agent in TNT) at room temperature followed, and then larvae were incubated with peroxidase-conjugated anti-digoxigenin-POD antibody (Roche 11 207 733 910) at 4°C overnight using a 1:400 dilution in TNTB. The next day, larvae were washed 8 times for 15 min each in TNT, stained for 1 hour in the darkness (Perkin Elmer TSA Plus Cyanine 3 System, NEL744001KT), and washed three times for 5 min each in TNT.

Paramecia consumption assay

Paramecia were stained as previously described (Jordi et al., 2015; Shimada et al., 2012), but using the 1,1'-Dioctadecyl-3,3,3′,3′-Tetramethylindodicarbocyanine, 4-Chlorobenzenesulfonate Salt (DiD') dye (ThermoFisher Scientific D7757). Cultured paramecia (approximately 100 mL) were purified by filtration through a fine mesh that retains them (pore size 20 μM), concentrated by centrifugation for 5 min at 3,000 rpm, and resuspended in 800 μL of water. The solid dye was dissolved in ethanol to make a 2.5 mg/mL working solution, of which 4 μL was added to the tube of paramecia. Paramecia were stained for 2 hours with gentle rocking, spun for 5 min at 3,000 rpm, washed two times with water, and resuspended in 1 mL of water. The food was used at approximately 100 μL for ten larvae, and the larvae in a 150 mm Petri dish were allowed to feed for 15 min before they were fixed in 4% PFA in PBS overnight. Prior to the assay, larvae had not eaten for over 12 hours. The next morning, larvae were rinsed three times in PBS and their stomach intensity was imaged on a Zeiss Axio Zoom.V16 Stereo Microscope with a Cy50 filter. Quantification was completed using the 3D objects counter in ImageJ with a constant threshold. All larvae are tested together and genotyped after imaging of stomach labeling.

Cell isolation and library preparation for 10X scRNA-seq

Cell isolation and capture in droplets was performed as previously described (Pandey et al., 2018) with the following minor modifications. Eight 6 dpf larval forebrains were dissected for each sample (wild-type and *znf536* homozygous mutant) in Neurobasal (ThermoFisher Scientific 21103049) supplemented with 1x B-27 (ThermoFisher Scientific 17504044) within approximately forty minutes. Forebrains were incubated in 20 units/mL papain (Worthington Biochemical Corporation LK003150) for 12 min at 37°C, followed by gentle trituration approximately 20 times and spinning at 300xg for 5 min. Dissociation was halted by resuspension in 1 mL of 1.1 mg/mL papain inhibitor in Earle's Balanced Salt Solution (EBSS), spun at 300xg for 5 min. The resulting pellet was then washed in Neurobasal supplemented with B27 before final resuspension in 50 μL PBS + 200 μg/mL BSA. To avoid cell loss, during each wash the supernatant was saved and spun a second time to recover cells. These cells were then mixed with the final cell suspension to increase cell count. After confirming a cell viability of greater than 80% using trypan blue, cells were counted on a hemocytometer and loaded onto the 10X Chromium system at a concentration of approximately 150 cells/μL. Libraries were prepared according to the manufacturer's instructions.

QUANTIFICATION AND STATISTICAL ANALYSIS

Brain activity and morphology analysis

Images were registered to a standard zebrafish reference brain using Computational Morphometry Toolkit (CMTK) (Jefferis et al., 2007; Rohlfing and Maurer, 2003). All phosphorylated-ERK images were normalized with a total-ERK stain. The Mann-Whitney U statistic Z score is calculated for each voxel, comparing between the mutant and control groups using MapMAPPING (Randlett et al., 2015). The significance threshold was set based on a false discovery rate (FDR) where 0.05% of control pixels would be called as significant. Structural analysis with CMTK was based on deformation-based morphometry (Cachero et al., 2010; Rohlfing and Maurer, 2003) to localize changes in brain volume, and the differences were calculated the same way as for the brain activity using MapMAPPING but with a 0.005% FDR threshold. When multiple comparisons were made, such as in the case of duplicated genes (Figure S4), the comparison with the most extreme phenotype was selected to represent the gene. The numbers of mutant and control fish in each experiment are available in Table S2 and on stackjoint.com/zbrain. All image processing and computational analyses were completed on the Harvard Odyssey cluster.

Image similarity analysis

To cluster the mutants based on their neural activities, the following steps were taken:

1 Calculated the absolute difference in pixel intensities between each mutant and its wild-type / heterozygous sibling control, as a measurement of neural activity changes in the mutant.

2 Set the pixels outside the brain region to zero intensity.

3 Defined each pixel with an intensity greater than 50 as a *signal* of activity change. The threshold of 50 was chosen such that background intensities were best separated from real signals based on test images.

4 If a brain activity imaging experiment was independently repeated (78 of the 132 mutants, 59 of those designated as having brain activity phenotypes), irreproducible signals were eliminated. First, the brains were segmented into four major brain regions: telencephalon, mesencephalon, rhombencephalon, and diencephalon (Randlett et al., 2015). Signals in a brain region were discarded if they occupied very few pixels (< 1/5000 of the total number of pixels in that brain region), or if they occupied pixels only in one of the two images. After the elimination of irreproducible signals, the two images were averaged to obtain one image for each mutant. These images were used for calculating pixel sums (Figure 1G, Figure 1H, Figure 4C).

5 Dilated each signal in 3D by 4-pixels in radius in x and y dimensions, and 2-pixels in radius in z dimension to define a *region* of activity change for each mutant (Equation 1).

6 For each pair of mutants, determined the *overlap* region of activity changes (Equation 3). Then, calculated the percentage of signals within the overlap region for each mutant and averaged the two percentages to obtain the similarity score between the two mutants (Equation 3).

7 Repeated step 6 for all mutant pairs to construct a similarity matrix, which was then used as the distance matrix for a hierarchical clustering algorithm.

$$region = signal * kernel \quad \text{(Equation 1)}$$

where *signal* is the binary 3D matrix that marks pixels with activity change with 1, * indicates convolution operation, and kernel is defined as:

$$kernel_{x,y,z} = \begin{cases} 1, & if \left(\frac{(x - r_x)^2}{r_x^2} + \frac{(y - r_y)^2}{r_y^2} + \frac{(z - r_z)^2}{r_z^2} \right) < 1 \\ 0, & otherwise \end{cases}$$

where rx, ry, and rz are the radius for dilation along the 3 dimensions.

$$overlap_{x,y,z} = region_{i_{x,y,z}} \times region_{j_{x,y,z}} \quad \text{(Equation 2)}$$

where $region_i$ and $region_j$ are regions of activity change for the i-th and j-th brain respectively, and x, y and z represent indices in the 3D matrices. The resulting *overlap* is a binary 3D matrix with 1 marking the overlapping pixels.

$$similarity_{ij} = \left(\frac{\sum_{x,y,z} signal_{i_{x,y,z}} \times overlap_{x,y,z}}{\sum_{x,y,z} signal_{i_{x,y,z}}} + \frac{\sum_{x,y,z} signal_{j_{x,y,z}} \times overlap_{x,y,z}}{\sum_{x,y,z} signal_{j_{x,y,z}}} \right) \Big/ 2 \quad \text{(Equation 3)}$$

Behavioral Analysis

For data with a time component (baseline movement frequency, features, and location preferences), a linear mixed effects model was used to calculate significance:

$$Movement \sim MutantorNot + Time + MutantorNot * Time$$

The model assumes that the movement of the fish can be approximated as a linear combination of (1) a constant (baseline) movement level, (2) a trend of movement in time, (3) a change in the baseline movement level due to the mutation, and (4) a change in the trend of movement due to the mutation. *MutantorNot* was the parameter evaluated for significance. The advantage of the linear mixed effects model is that it takes into account the longitudinal order of the data points, and therefore has the potential of recognizing consistent changes within a limited time window that might be missed if the order is disregarded. The more simplistic mean value and variance measures are available in Dataset S1, but are an inaccurate representation of data that changes in magnitude over time. Kruskal–Wallis one-way ANOVA was used to compare stimulus responses for mutant and control groups based on the mean response metric for each fish. Using p values allowed the identification and comparison of statistically significant phenotypes across diverse behavioral assays, some of which required the linear mixed model for accurate significant determination and others that could be assessed with a standard Kruskal-Wallis test. The accuracy of comparing mutant effect sizes across assays, such as by using strictly standardized mean difference (SSMD), is limited for such diverse behaviors because the calculation depends on mean and variance values for baseline movement data.

Once significance was determined for individual metrics (listed below) the p values were merged into 71 categories or behavioral assays as described in Figure S2B and Figure S2C. The p value merging was necessary to reduce false-positive phenotypes. Multiple similar metrics associated with one of the 71 behavioral assays had to be statistically significant before the mutant was considered to have a phenotype. Multiple similar metrics had to be be statistically significant before the mutant was considered to have a phenotype. For example, ''number of bouts per minute'' and ''active minutes per 10 minute'' are both ''Frequency of movement'' metrics, and more than three such metrics had to be significant to designate a ''Frequency'' phenotype. The merging approach was empirically defined as giving a < 10% false discovery with randomized batches of wild-type larvae (Figure S2C). We have provided one annotated example of all individual metrics and the merged final p value (Table S3).

Alternative behavioral data analyses, such as the SSMD, can be conducted using Dataset S1 and scripts available in the github repository associated with this manuscript. We also developed a procedure to describe potential shared phenotypes between the brain activity and behavioral datasets (Figure S7), and those scripts are available on github. We chose this approach in order to connect activity changes in specific brain regions to a corresponding behavioral output. This approach was more fruitful than comparing clustering results of the two datasets, because mutants do not form clusters sharing behavioral phenotypes in all assays even though they do share phenotypes in subsets of assays (Table S4, Figure S7).

Behavioral metrics

Movement frequency metrics (12): Number of bouts (based on distance) / min, Number of bouts (based on distance) / 10 min, Number of bouts (based on delta pixels) / min, Number of bouts (based on delta pixels) / 10 min, Active seconds / min (based on distance), Active minutes / 10 min (based on distance), Active seconds / min (based on delta pixels), Active minutes / 10 min (based on delta pixels), Average interbout interval (seconds) / min (based on distance), Average interbout interval (seconds) / 10 min (based on distance), Average interbout interval (seconds) / min (based on delta pixels), Average interbout interval (seconds) / 10 min (based on delta pixels). A ''bout'' is a movement that passes certain threshold parameters, and it can be calculated based on either change in pixels between frames (threshold of 3 frames and 3 pixels) or based on actual distance moved in pixels (threshold of 2 frames and 0.9 pixels). The ''interbout'' is the time between movements.

Movement features metrics (14): Average bout cumulative delta pixels (pixels) / min, Average bout cumulative delta pixels (pixels) / 10 min, Average bout distance (pixels) / min, Average bout distance (pixels) / 10 min, Average bout displacement (pixels) / min, Average bout displacement (pixels) / 10 min, Average bout time (milliseconds) / min (based on distance), Average bout time (milliseconds) / 10 min (based on distance), Average bout time (milliseconds) / min (based on delta pixels), Average bout time (milliseconds) / 10 min (based on delta pixels), Average bout speed (pixels / millisecond) / min, Average bout speed (pixels / millisecond) / 10 min. Average bout velocity (pixels / millisecond) / min, Average bout velocity (pixels / millisecond) / 10 min. An increased or decreased mutant response (blue or yellow in heatmaps, Figure 2) in features of movement depends on what metric is most significantly different. It is feasible that a mutant could have decreased speed and increased distance.

Location in well metrics (8): Fraction of bout time in well center / min, Fraction of bout time in well center / 10 min, Fraction of interbout time in well center / min, Fraction of interbout time in well center / 10 min, Average bout rho / maximum rho / min, Average bout rho / maximum rho / 10 min, Average interbout rho / maximum rho / min, Average interbout rho / maximum rho / 10 min. The value rho is the radius in polar coordinates, used to determine location in well.

Stimulus metrics (15-148, depending on number of sections combined, e.g. weak taps occur before the strong tap in prepulse and also independently, measures for both are merged): Frequency, Latency (milliseconds), Displacement (pixels), Cumulative distance (pixels), Area moved (pixels) (Figure 2E), Time (milliseconds), Speed (pixels / millisecond), Velocity (pixels / millisecond), Cumulative delta pixels, Peak change in delta pixel per response (pixels), Peak speed in per response (pixels / millisecond), Maximum change in delta pixels from average response trace (delta pixels in every frame), Location of maximum change in delta pixels (millisecond), Maximum change in distance from average trace (distance in every frame), Location of maximum change in distance (millisecond). In addition to all the parameters described, all tap responses were further analyzed based on the same parameters for two subsets of responses: canonical escapes and weaker responses that follow if the larva did not escape. ''Big'' responses (e.g. true escapes) were designated as having a velocity of >0.2 pixels / millisecond and having a latency of less than 25 millisecond from the start of recording (not from the actual tap occurrence). These parameters were determined by analysis of responses to the strong tap, which are true

escapes the vast majority of the time. The ''small'' responses were every other response that occurred up to 75 milliseconds after the start of recording. All frequency phenotypes for prepulse inhibition experiments shown in Figure 5D represent changes in frequencies for ''big'' responses (true escapes). An increased or decreased mutant response (blue or yellow in heatmaps, Figure 2) in stimulus responses depends on what metric is most significantly different. It is feasible that a mutant could have increased response frequency with decreased distance.

Analysis of single-cell sequencing data

First, cells were filtered to remove those that contained less than 200 genes and those in which > 6 of transcript counts were derived mitochondrial-encoded genes. Similarly, genes detected in less than 5 cells were removed. All cells derived from regions other than the forebrain, such as habenula and olfactory bulb, were removed. Similarly, non-neuronal types such as microglia and vascular cells were also removed from further analysis. The residual matrix was then scaled, centered and used for further analysis.

To select highly variable genes, we used a combination of a UMI based method described recently (Pandey et al., 2018) and Seurat's (Satija et al., 2015) variable gene selection approach. The resulting expression matrix across the highly variable genes was then used to perform dimensionality reduction and clustering using Seurat.

To compare signatures between mutant and wild-type datasets, both datasets were independently clustered as described. We used a multi-class Random Forest Classifier (Breiman, 2001) exactly as described in (Pandey et al., 2018). Briefly, the classifier was built on the most variable genes across both datasets using 1000 trees with R package RandomForest. The classifier was trained on 70% of the wild-type dataset and tested on the remaining 30% of the cells (Figure S6C). Each cell in test set was only assigned into a label if a minimum of 13% of the trees in the forest converged onto a decision. Otherwise the cells were unassigned. The resulting classifier was then used to predict wild-type labels for the cells in the mutant dataset.

DATA AND SOFTWARE AVAILABILITY

All mutants have been cryogenically preserved as sperm, and are available upon request. All raw behavioral and imaging data are available upon request. A zip archive of files containing metric p values and merged p values (similar to Table S3) is provided for every behavioral run (Dataset S1). Additional files containing the mean, variance, N, and unprocessed p value for control and mutant metrics are also provided (Dataset S1). Metric data used to generate these statistics can be downloaded from the following site: https://zenodo.org/record/2522485#.XCAmmRNKh24, and has been issued the DOI 10.5281/zenodo.2522485. All graphs and analyses in this manuscript can be replicated from this dataset. The 10X raw sequencing data has been deposited in GEO under the codes GSE115427. Labview code for tracking larvae and generating high-speed movies is available from the Harvard CBS Neuroengineering core at https://github.com/cbs-ntcore/Schier-Lab. Code for analyzing high-speed movies, processing both slow- and high-speed tracking data to generate behavioral graphs, generating alternative analyses of behavioral data, and for clustering brain activity maps are available at

https://github.com/sthyme/ZFSchizophrenia. Code for calculating larvae locations and changes in pixels per frame (delta pixels) in high-speed stimulus response movies is partly based on previously published python tracking code (Conklin et al., 2015).

Additional Resources

All mutant allele information is available on the following website:

genepile.com/scz_gwas108

This website also includes select (5-14) behavioral graphs (raw metrics) for each mutant. Five graphs are the same for all mutants, and then up to nine graphs are included for each of the 73 mutants that were tested at more than once. These nine graphs represent the lowest p value metric contributing to the reproducible phenotypes (Figure 2G) for each of these mutants.

Imaging data for mutants are available on the following website:

stackjoint.com

stackjoint.com is a community resource, where users can upload their own data and share it with a limited set of colleagues or make it publicly available. Images can be hosted from any location chosen by the user. Any stack of images (any size, resolution, or number) can be shared through this site on stackjoint.com/basic, and zebrafish data that is registered to the Z-Brain can add to a growing repository of 6 dpf zebrafish neuroimaging data on stackjoint.com/zbrain. Users can upload and analyze their own zebrafish brain activity maps to identify regions of altered signal, based on Z-Brain anatomical masks available in this online resource. Colors of differences maps (activity, structure, or any antibody stain of interest) are designated as green for increased signal in test group (gene mutant, drug, or stimuli) and magenta for decreased. The current map naming convention for mutant data is *Gene_AnalysisType_NofComparedAnimals_ExperimentalInfo_RunNumber_SignificanceCutoff*

e.g., ambra1_structure_13homhomover31homhet_hethomfxhomhetm_2nd_p00005

where analysis type could be any antibody name, drug or stimuli type could replace gene name, and experimental information could be anything of relevance such as concentration of a drug. If uploading large amounts of data to this site, please contact for assistance in streamlining the process.

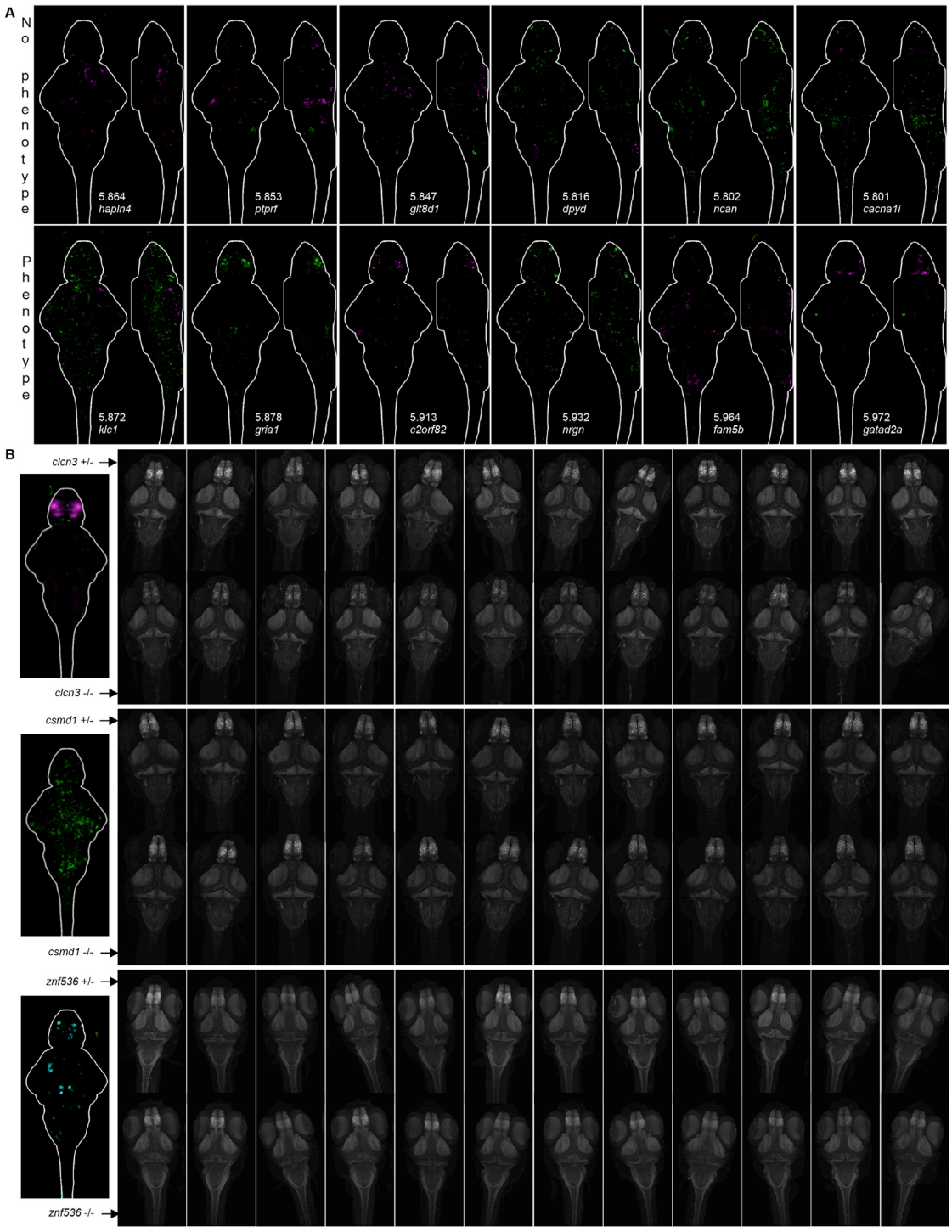

Figure S1. Defining Imaging Phenotypes, Related to Figure 1, Figure 3, Figure 4

(A) Determination of cutoff for brain activity signals. Images are sum-of-slices intensity projections (Z- and X- axis). This cutoff for the $\log_{10}$(sum of pixels) was made so that mutants with small, specific, repeatable signals were classified as having phenotypes (*gria1,* forebrain). Full stacks of all individual repeats are available on stackjoint.com/zbrain. Many mutants with diffuse and sparse signals (likely noise) fell below the cutoff. Exceptions included *klc1* and *nrgn* (shown here), which both had signals that reproduced in independent experiments (stackjoint.com/zbrain).

(B) Examples of individual homozygous mutant and heterozygous control brains stained with phospho-Erk (*clcn3*, *csmd1*) or total-Erk (*znf536*) (maximum intensity projections). Twelve brains of each genotype are shown for the three genes. The localized reduction in forebrain activity observed in the *clcn3* map is readily observable in the original images. In contrast, the widespread increased activity in the *csmd1* map is not as discernable by eye, but is still noticeable in some areas

(legend continued on next page)

(mesencephalon, rhombencephalon). The MapMAPPING protocol (Randlett et al., 2015) quantifies these less obvious differences. Significant voxels are defined using the Mann-Whitney U statistic Z score, intrinsically selecting for repeatable signals. Variability in brain activity between individuals is most likely due to subtle differences in the experiences of the larvae during the last ten minutes before fixation (the integration time of phospho-Erk). Structural changes in *znf536* mutants are discernable for the smaller size of the forebrain pallium and symmetric reduction in the cerebellum. The other small signals are likely noise, as they are asymmetric (Figure 3B; *znf536* is in the "small changes and noise" group).

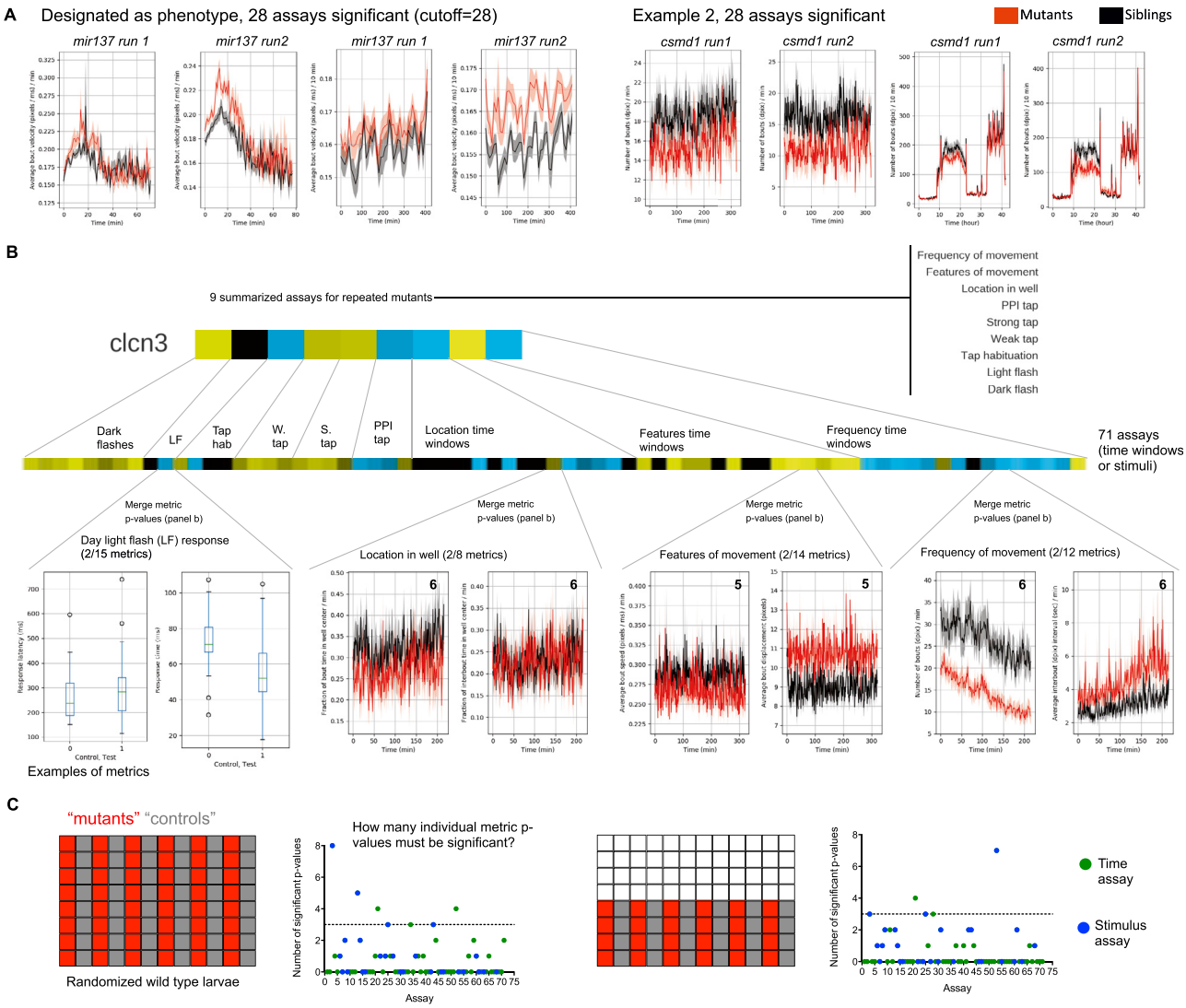

Figure S2. Quantification and Analysis. Defining Behavioral Phenotypes, Related to Figure 1, Figure 2, STAR Methods

(A) Determination of cutoff for the number of behavioral assays with a significant (< 0.05) p value. A total of 71 assays were analyzed (Figure 2, STAR Methods). The mutant *mir137* was chosen as the lower end of the cutoff, having a significant phenotype in 28 of the 71 assays. This mutant has a repeatable increased velocity of motion, shown here for two time windows: heat stressor and dark flashes. A second example of a mutant at the cutoff is *csmd1*, which has a repeatable reduction in frequency of movement (shown here with day taps time window and entire assay). Data is expressed as mean ± SEM. Avoiding falsely designating a mutant as having a phenotype required determining a cutoff for the number of assays (out of 71) that must be significant (28). Our goal was a false-discovery rate of less than 10%, where 7 or less of the 71 assays would be significant false-positives for any comparison. However, multiple comparisons were performed for duplicated genes and when two heterozygous parents were crossed (i.e., homozygous larvae were compared both to heterozygous and to wild-type). Therefore, to correct for multiple comparisons we increased the cutoff to four times higher (28). This stringent cutoff may result in false negatives, but was confirmed to define mutants with specific and repeatable differences, such as shown here, as having a phenotype.

(B) The 71 assays (described in detail in the STAR Methods) included Frequency of movement, Features of movement, and Location in the well for each of the 14 time sections and full 2-day assay, for a total of 45 baseline assays. The remaining 26 assays were stimulus-driven: prepulse, weak, and strong taps during the night and day (12 assays), tap habituation (4 assays, 3 day and one night), light flashes (2 assays, one day and one night), and dark flashes (8 assays; 4 blocks, beginning and end ten flashes analyzed separately). Each of the p values in the 71 assays is based on multiple "metrics," which were merged to determine significance. Multiple metrics were required to be significant for the entire assay to achieve significance (see C). Two examples of each type of metric are shown for each of these assay types, and all metrics are described in the STAR Methods. One complete example of the output of the merging procedure is available in Table S3, with p values for the merged dataset and p values for each individual metric. These p values for the 71 assays do not take reproducibility across independent experiments into account (the lowest p value of all comparisons and experiments is shown). Reproducibility was accounted for in the dataset of 46 mutants that were tested more than once and were designated as having a phenotype (Figure 2G). If two runs had a significant p value in the same time window or same stimulus assay of the 71 tested assays, then the phenotype was considered reproducible and nine final values were generated.

(legend continued on next page)

(C) Significance in each of the 71 assays required that multiple contributing and similar metrics (raw data) were significant. We determined how many individual metrics in an assay must be significant for the assay (of the 71 assays) to be scored as significant by comparing randomized groups of wild-type larvae. Three separate batches of wild-type larvae were put through the standard behavioral protocol and analysis. Three comparisons were conducted for each of the three batches (two comparisons with a total of 48 larvae and one with 96). Based on all nine wild-type larvae comparisons, we determined that if more than three (gray dashed line) individual p value metrics were significant, then less than 10% of 71 assays would be false positives. The merged p values for stimulus response (blue points) included many more metrics than Frequency, Features, and Location (green points) making them more prone to false positive outcomes. These assays represent close to half of the false positives, while they make up 1/3 of the assays (26/71). To further minimize such false positives in the stimulus response assays, the threshold was set to > 4 with the exception that it would be reduced to > 2 in the case that the exact same metric (e.g., velocity) were significant across two related assays (e.g., light flashes at night and during the day). This reduction in the cutoff was important because highly specific phenotypes, such as changes only in the latency of the dark flash response, were designated as non-significant when the cutoff value was set to 4.

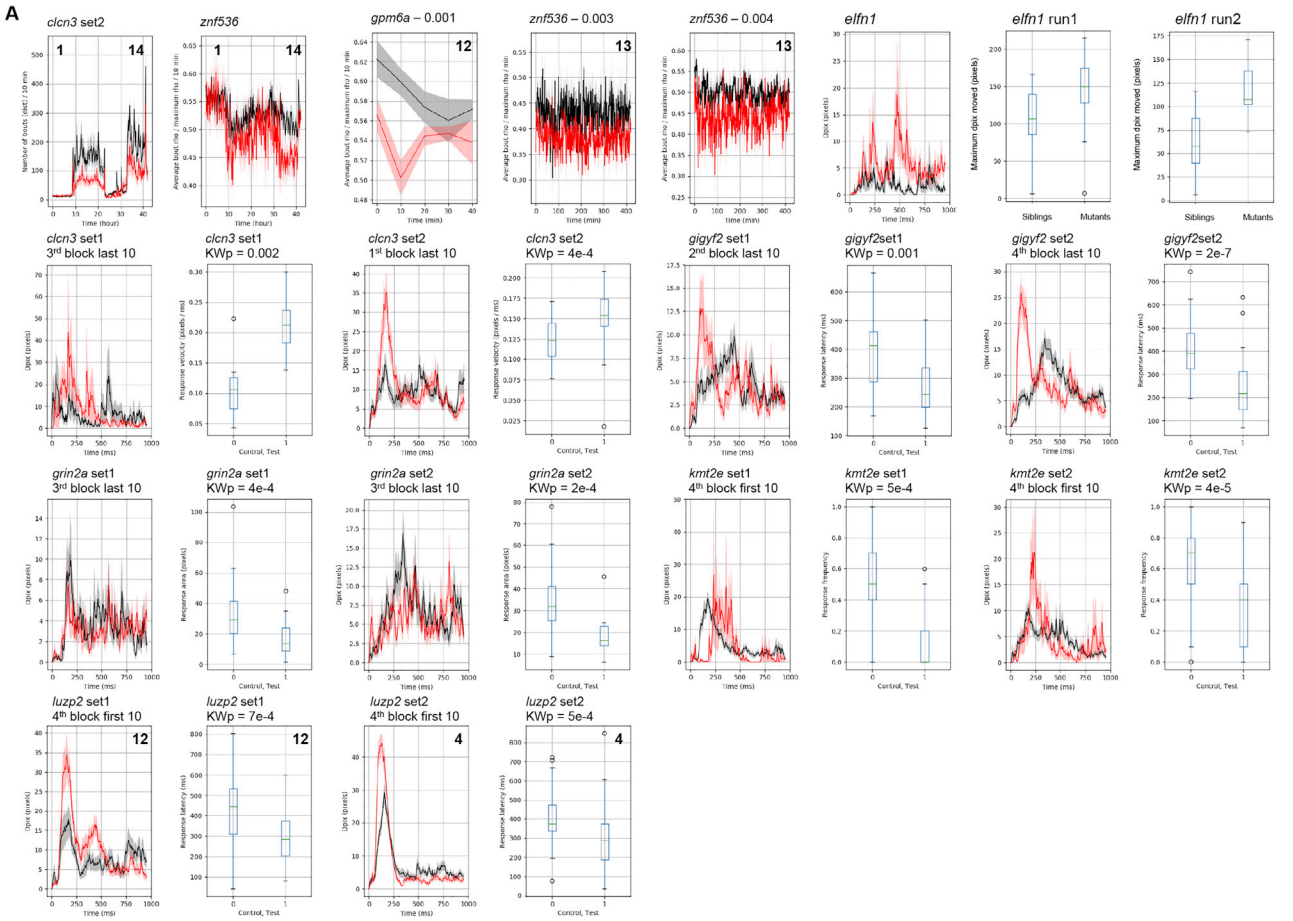

(legend on next page)

Figure S3. Supporting data for Figure 2 and Figure 5 Behavioral Plots, Related to Figure 2, Figure 5

(A) Repeats for behavioral data in Figure 2. This includes the plots for the heatmap of mutants with altered dark flash responses (Figure 2E). In Figure 2E, the significance for 8 sections of dark flash analysis were combined with Fisher's method. Here, the most significant section is shown, with the p value from Kruskal-Wallis one-way ANOVA. The movement trace for the response is the mean ± SEM for ten flash events. For the data that is not stimulus-driven, the p values are calculated using the linear mixed model.

(B) Repeats for behavioral data in Figure 5. This includes mutants with prepulse inhibition phenotypes from the heatmap in Figure 5D. Boxplots and associated Kruskal-Wallis one-way ANOVA p values are shown for one modality of response that repeated across two assays. The movement trace for the response is the mean ± SEM for prepulse tap events (strong tap after the weak; specifically counting only responses designated as "big moves," see STAR Methods).

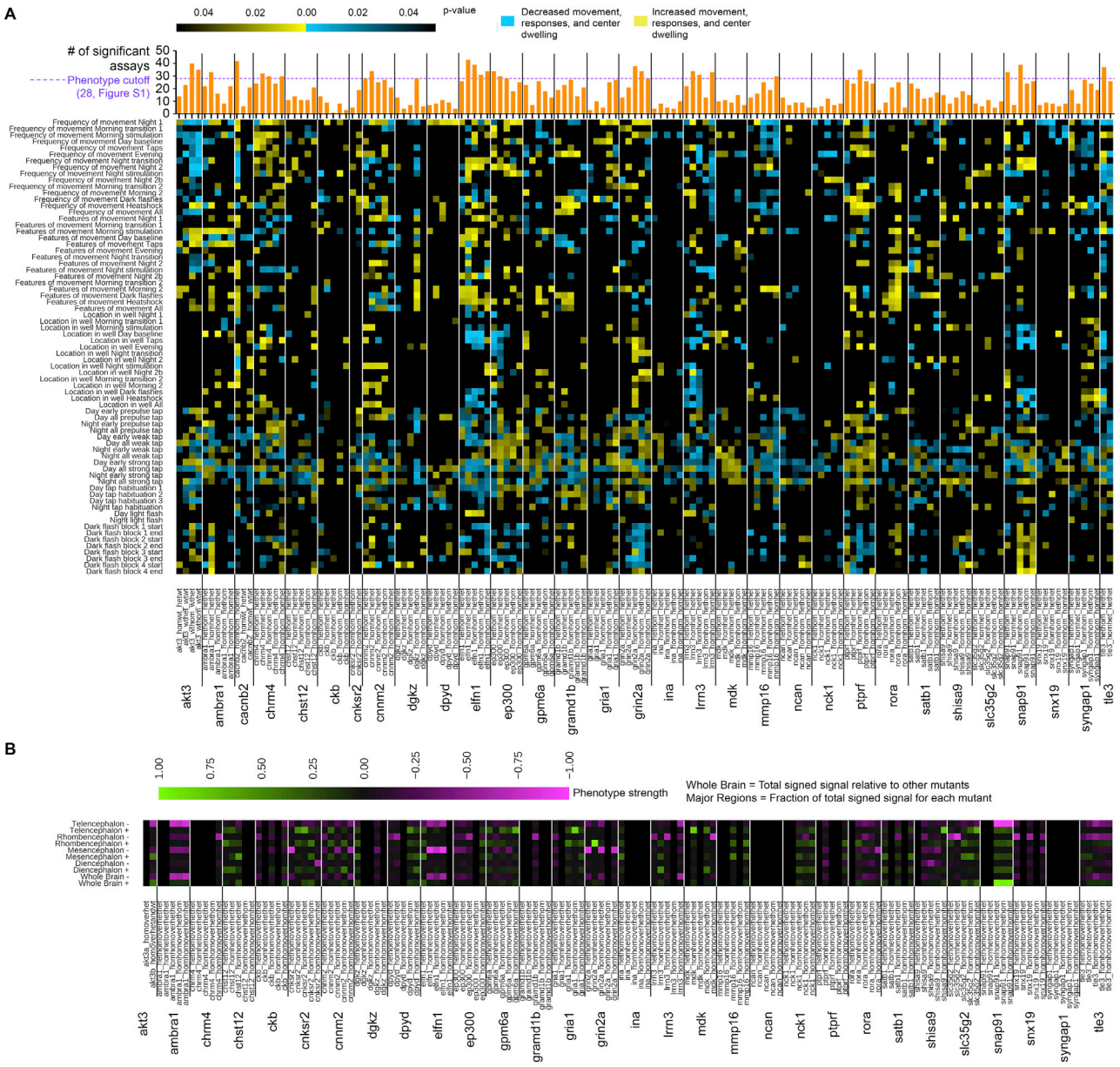

Figure S4. Phenotypes for Individual Orthologs of Duplicated Genes, Related to Figure 2 and Figure 4

Of the 132 mutated genes, 33 had two orthologs that were both mutated (Table S2). The x axis label of the heatmap describes the genotypes being compared in each column; e.g., homhom corresponding to (-/-;-/-) or hethet corresponding to (+/-;+/-). The majority involve 5 comparisons because the parent crosses were either homhom x hethet or homhet x hethom. A small minority included less than 5 comparisons due to experimental limitations.

(A) Behavioral phenotypes, as described for Figure 2F for 31 of the 33 duplicated genes. If a mutant was repeated, the lowest combined p value is shown here. The two mutants that were generated but not tested were *foxg1b* and *bcl11bb* because *foxg1a* and *bcl11ba* were found to have extremely strong (and lethal) phenotypes, and assays were completed with the "b" alleles as homozygous in the background of the "a" allele comparisons. We presume that the "a" orthologs of these two genes have more conserved functions, as their phenotypes resembled mammalian knockouts (Figure 3C).

(B) Brain activity phenotypes, showing the signal in each of the four major brain regions with the color corresponding to the direction of the activity change in the brain activity maps. Prior to dividing the signal in each region by the total signal, the regions were scaled relative to each other based on their respective sizes (rhombencephalon = *1, diencephalon = *1.76, mesencephalon = *1.42, telencephalon = *4.36). The original whole brain signal was separately scaled across all mutants with a phenotype, indicating the relevance of the signal in each of the regions. Thirty of the 33 duplicated genes are included in the analysis, as *bcl11b* and *foxg1* are missing (see panel A) and *cacnb2b* was identified as the ortholog with the much stronger (and lethal) phenotype compared to *cacnb2a*.

Figure S5. Comparison between *in situ* RNA Localization and Brain Activity, Related to Figure 4

Stacks of all RNA-FISH images are available on http://stackjoint.com/basic/ and are tagged as "Thyme, 2018." Probe sequences are available on http://genepile.com/scz_gwas108. At least three brains were imaged for each probe to confirm that the presented pattern was consistent (data available upon request). Brain area descriptions are based on the Z-Brain masks (stackjoint.com/zbrain). *znf536:* forebrain showed *in situ* and phosphorylated-Erk (pErk) brain activity signal. *grin2aa*: cerebellum showed *in situ* and activity signal. *elfn1a:* retinal arborization field AF7, tectum, and forebrain showed *in situ* and activity signal. *foxg1:* forebrain showed *in situ* and activity signal. *gria1a:* forebrain showed *in situ* and activity signal. *cacna1c:* cerebellum and forebrain showed *in situ* and activity signal. *hcn1:* hindbrain showed *in situ* and activity signal. *egr1:* forebrain showed *in situ* and activity signal. *roraa:* tectum and hindbrain showed *in situ* and activity signal. *nrgn:* forebrain and hypothalamic cells showed *in situ* and activity signal. *snap91:* activity signal correlated to *in situ* signal showing expression throughout the brain. *shisa9b:* forebrain showed *in situ* and activity signal. *znf804a:* activity signal correlates to *in situ* signal showing expression throughout the

(legend continued on next page)

brain. *lrrn3:* activity signal correlated to *in situ* signal showing expression throughout the brain. *csmd1*: activity signal correlated to *in situ* signal showing expression throughout the brain. *cnnm2b:* strong *in situ* signal in forebrain and torus semicircularis did not correlate to activity signal in tectum, retinal arborization field AF7, and hindbrain. *csmd3:* strong *in situ* signal in retinal arborization field AF7, tectum, and hindbrain did not correlate to diffuse and minimal activity signal. *tcf4:* strong *in situ* signal in forebrain and midbrain did not correlate to strong activity signal in tectum. *luzp2:* Strong *in situ* signal in tectum and cerebellum did not correlate to activity signal in hindbrain. *tle3a:* strong *in situ* signal in forebrain and tectum did not correlate to strong activity signal primarily in hindbrain. *clcn3:* strong *in situ* signal throughout the brain did not correlate to activity signal mainly in forebrain. *grin2ab:* strong *in situ* signal throughout the brain did not correlate to activity signal primarily in the tectum, retinal arborization field af7, and hindbrain. *bcl11b:* strong *in situ* signal throughout the brain did not correlate to activity signal in forebrain and cerebellum.

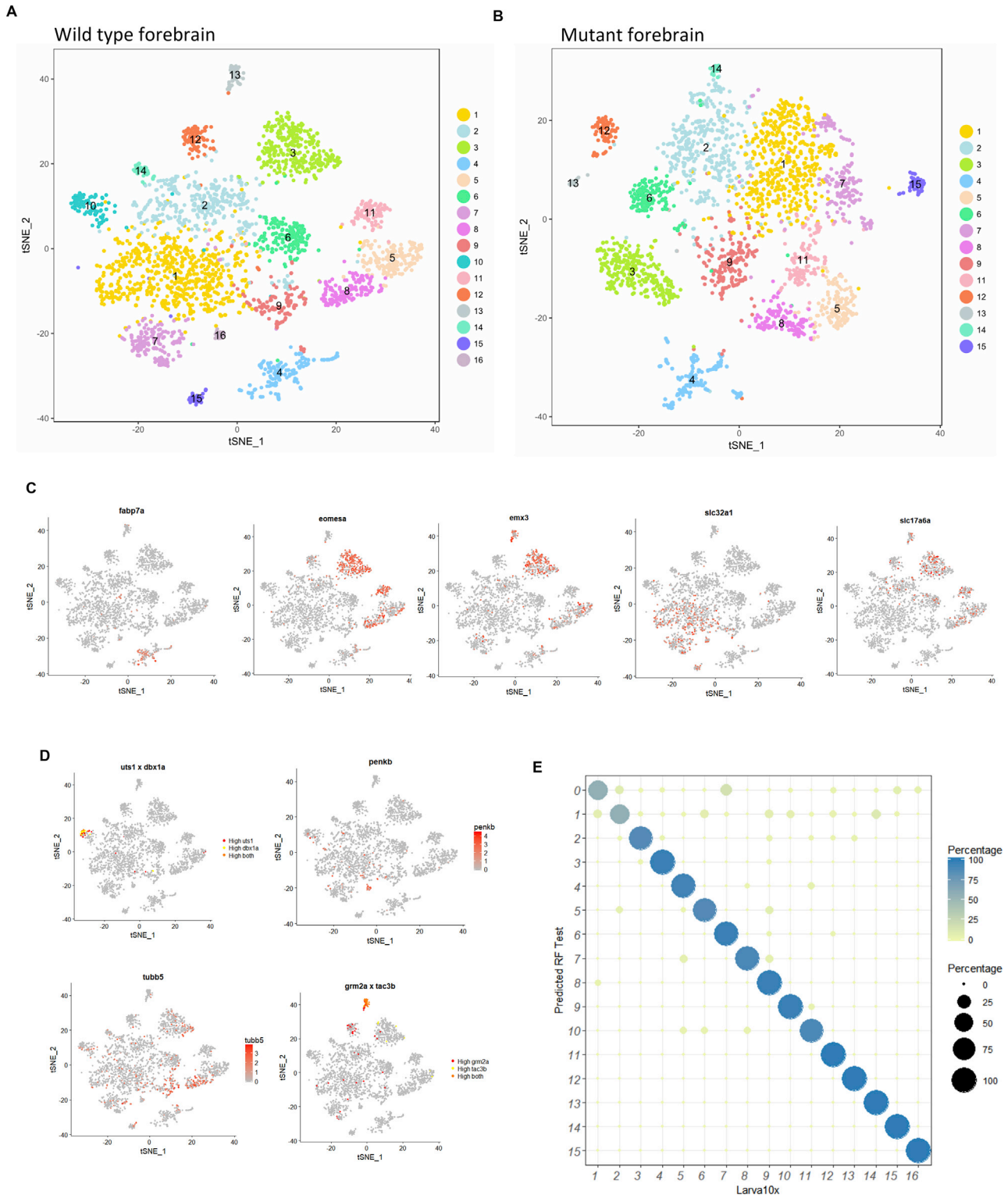

Figure S6. Single-Cell Analysis of *znf536* Mutant and Wild-Type Forebrain Cells, Related to Figure 6

(A) 2D visualization of single-cell clusters in the wild-type dataset using t-distributed stochastic neighbor embedding (t-SNE). Individual points correspond to single cells and are color coded according to their cluster membership determined by graph-based clustering.

(B) 2D visualization of single-cell clusters in the *znf536* mutant dataset using t-SNE. Mutant clusters are color-coded and labeled according to their correspondence to wild-type forebrain clusters.

(legend continued on next page)

(C) Gene expression profiles of key forebrain marker genes across the wild-type dataset.
(D) Gene expression profiles of marker genes of clusters that are 1) missing in mutant: (Cluster 10: *uts1* and *dbx1a* and Cluster 16: *penkb*) 2) reduced in mutant (Cluster 13: *grm2a* and *tac3b*) or 3) increased in mutant (Cluster 9: *tubb5*), a marker for immature neurons.
(E) Performance of random forest (RF) model trained on the wild-type dataset with graph clustering labels shown in Figure S6A. Training set was formed by choosing 70% of the cells from wild-type dataset, with proportional representation from each cluster. The trained RF model was used to classify cells in the remaining (test) dataset. The resulting classification of the test set is shown as a confusion matrix. Cells are either assigned into their corresponding labels or left unassigned if they cannot be reliably assigned to any of the training labels.

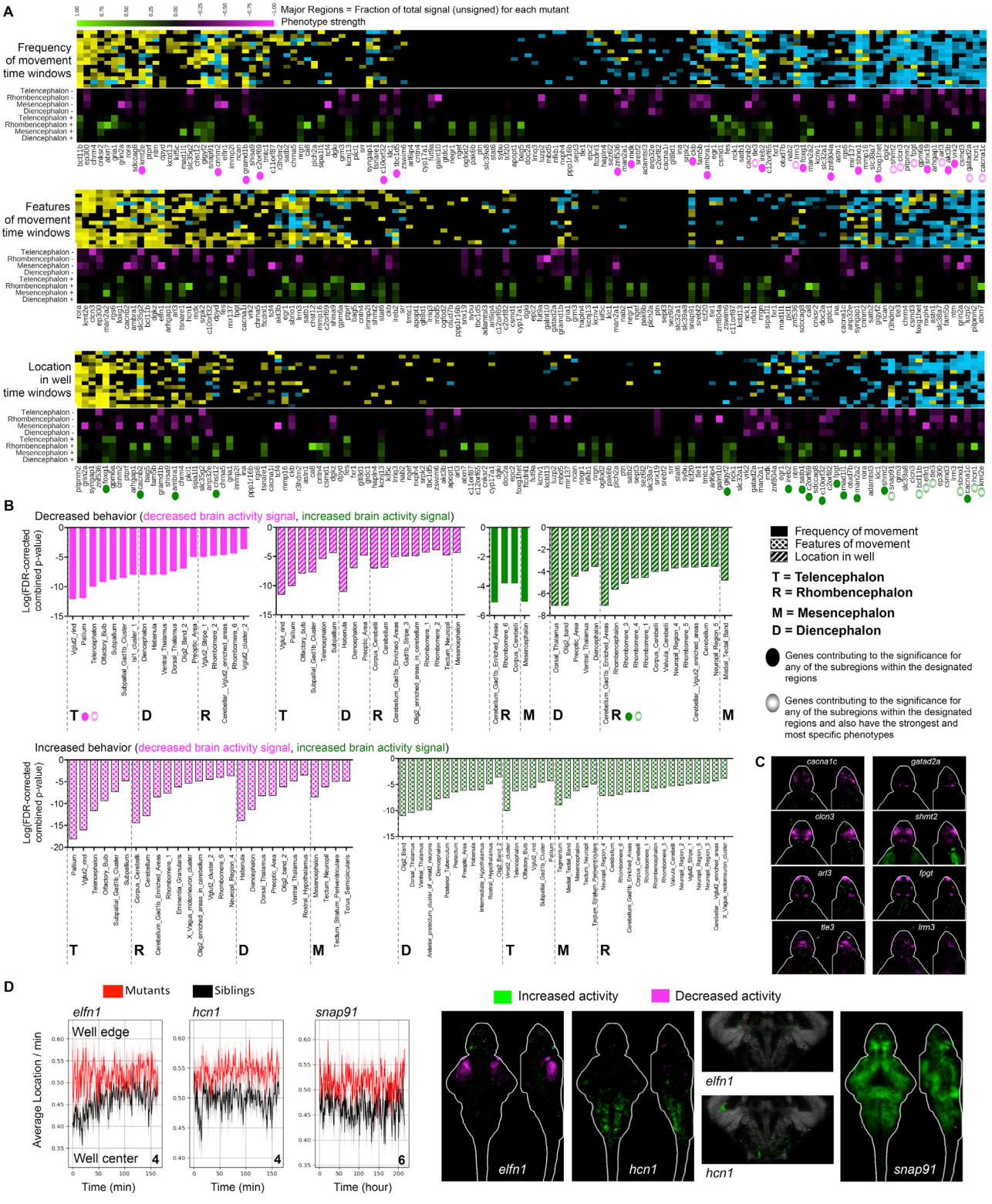

Figure S7. Comparison of Brain Activity and Behavioral Datasets, Related to Figure 2 and Figure 4

(A) Comparison of baseline behavioral data across multiple time windows (Figure 2) with brain activity changes in the four major regions. Stimulus-driven behaviors (prepulse, dark flash response, etc) are not comparable to the baseline phospho-Erk data. There are several caveats to consider when comparing these two datasets. The behavioral data was collected on larvae in 96-well plates, isolated from interaction with any other larvae and constrained in their movement,

(legend continued on next page)

while phospho-Erk staining was completed on a group of larvae in a large (150 mm) Petri dish. It is likely that the differences in these conditions would result in different brain states. The phospho-Erk dataset also represents only a single time point, the afternoon of 6 dpf, while the behavioral data was collected across two nights and days. Both the phospho-Erk and behavioral analyses only explore a small and relatively non-overlapping part of the possible behavioral landscape, and a more appropriate assessment would be to compare these two types of data collected under the same conditions for specific behaviors of interest. Further, finding similar differences in brain activity in a region does not necessarily mean that the exact same neurons are affected.

(B) To search for connections between brain activity and behavior in an unbiased and quantitative way, we developed a procedure to compare the merged p values from baseline behavioral assays with the region-specific brain activity signal. Two relationships remained convincing after qualitative assessment (open circles) of the results: a relationship between reduced frequency of motion and a reduced activity in the telencephalon (C), and a relationship between increased activity in the rhombencephalon and increased preference for the well edge (D). Briefly, we binarized both the brain activity and behavioral data and conducted Fisher exact enrichment analyses, followed by combining the resulting p values for all time windows to look for relationships that were consistent across time and therefore more likely real. For the brain activity data, we focused on the 61 largest regions based on their size in pixels, and normalized the total number of pixels with signal by dividing by the region size. Regions with less than 1% activity were designated as 0 and regions with greater than 1% signal were designated as 1. This binarization was not optimal and certainly resulted in false positive designations of signal (filled-in circles represent contributions to quantitative significance that were potentially false designations, compared to open circles where binarization more accurately represented the data). For the behavioral data, any assay with a significant merged p value (< 0.05) was designated as 1. Following initial enrichment analyses across a matrix of the 61 regions and 45 baseline time windows, the resulting Fisher p values were combined across the time windows using Fisher's method. The most significant combined p values are shown for the comparisons of both increased behavior and decreased with increased and decreased binarized brain activity signal. If a comparison is not shown, no combined p values of substantial significance were identified.

(C) Brain activity maps for the forebrains of eight mutants that have both convincing telencephalon activity reductions and a consistent reduction in baseline frequency of motion (open circles, A).

(D) Three examples of mutants with an increased preference for the well edge. Correspondingly, we observed substantial increases in brain activity in these mutants, specifically in the hindbrain region for *elfn1* (see also Figure S5 brain activity map for only *elfn1a*) and *hcn1*. Additional examples are highlighted with open circles (A) and are available to view as stacks on stackjoint.com/zbrain. Intriguingly, several of these mutants have also been implicated in epilepsy (references in Table S1), another neuropsychiatric disease that may share genetic underpinnings with schizophrenia.